RESEARCH ARTICLE

VOLCANICA

Pumice cone eruptions at Aluto volcano, Ethiopia

Ben Clarke*[α,β,ϒ], Eliza S. Calder[ϒ], Karen Fontijn[δ], Firawalin Desalegn[ε], Pablo Tierz[ζ,ϒ,η], and Gezahegn Yirgu[θ]

[α] Earth Observatory of Singapore, Nanyang Technological University, Singapore, 639798, Singapore.
[β] School of Geography, Geology and Environment, University of Leicester, Leicester, UK.
[ϒ] School of Geosciences, University of Edinburgh, King's Buildings, Edinburgh, UK.
[δ] Department of Geosciences, Environment and Society, Université libre de Bruxelles, Brussels, Belgium.
[ε] CNCS, Wollega University, Nekemte, Ethiopia.
[ζ] British Geological Survey, The Lyell Centre, Edinburgh, UK.
[η] Geociencias Barcelona (GEO3BCN), CSIC, Barcelona, Spain.
[θ] School of Earth Sciences, Addis Ababa University, Addis Ababa, Ethiopia.

Submitted: 2023-09-15 | Accepted: 2024-09-13 | Published: 2024-11-12

Editor: J Farquharson | Typesetter: J Farquharson

Abstract

Pumice cones are volcanic landforms that exist worldwide, but whose eruption has never been observed. Interpretations of these eruptions vary significantly in style, intensity, and magnitude, pertinent for volcanic hazard assessment. Aluto volcano (Ethiopia) provides an unprecedented insight into the hazardous nature of these enigmatic eruptions. We investigate nine such pumice cones, and find that they are the product of moderate-intensity explosive eruptions that develop a sustained but unsteady eruption column, deposit lapilli- to block-sized tephra close to the vent forming pumice cones, can deposit distal tephra from an umbrella cloud, produce pyroclastic density currents by repeated partial column-collapse, and end with the emplacement of silicic lava. Like basaltic pyroclastic cones, pumice cones can also undergo collapse by lava flow emplacement. Alongside recent evaluation of distal tephras, we suggest that these eruptions, at least at Aluto, vary in intensity and magnitude from violent-Strombolian to sub-Plinian, and each follow a remarkably similar sequence of eruptive processes.

ምጥን ፅሁፍ

የሆፊ ሾጣጣ ኮረብቶች በመላው አለም የሚገኙ በእሳተገሞራ ፍንዳታ የሚፈጠሩ መልክዓ ምድራዊ ቅርፆች ሲሆኑ የፍንዳታቸው ክስተት ግን በጭራሽ ታይቶ አይታወቅም። የእነዚህ ፍንዳታዎች ትርጓሜዎች በአፈጣጠራቸው ዘይቤ (እስታይል) ፣ ጥንካሬ (ኢንተንሲቲ) እና መጠን (ማግንቲዩድ) በጉልህ ይለያያሉ፤ ይህም ለእሳተ ገሞራ አደጋ ግምገማ ጠቃሚነት አለው። በኢትዮጵያ የሚገኘው የአሉቶ እሳተ ገሞራ ስለእነዚህ እንቆቅልሽ ስለሆኑ ፍንዳታዎች አደገኝነት ከዚህ በፊት ያልተገኘ አዲስ ግንዛቤን ያስጨብጣል። እንደዚህ ያሉ ዘጠኝ የሆፊ ሾጣጣ ኮረብቶች ያጠናን ሲሆን ግኝታችንም የሚከተለው ነው። ሆፊዎቹ መካከለኛ ጥንካሬ ያለዉ የሀይለኛ እሳተ ገሞራ ፍንዳታ ውጤቶች ሲሆኑ፤ ፍንዳታውም ያልተቋረጠ ግን ያልተረጋጋ የፍንዳታ አምድ ወደ ሰማይ በመፍጠር፤ ከመካከለኛ እስከ ትላልቅ መጠን ያላቸው ውርውር ቅልጥአለት ድንጋዮች በእሳተገሞራ መውጫው ዙሪያ በማዝነብ ሾጣጣ ኮረብቶች ይፈጥራል፤ የፍንዳታው አምድ ጣሪያው ክፍል ዝንጥላ መሳይ የብነ-ገሞራ ደመና ዘርግቶ በነፋስ አቅጣጫ ርቀት ከተጓዘ በኋላ ወደ መሬት ተመልሶ በመዝነብ የብነ-ገሞራ ክምችት (ቴፍራ)ን ሊፈጥር ይችላል፤ ወደ ሰማይ የተምዘገዘገው ከፊል የእሳተገሞራው አምድ በተደጋጋሚ ተደርምሶ የተለያየ መጠን ያላቸው የቅልጥአለት ፍርክሶች በደቃቅ ብነ-ገሞራ ውስጥ ታቅፈው እንደ ፈሳሽ በስበት ሀይል የሚንቀሳቀስ ጎርፍ (ጅረት) ይፈጥራል፤ በማስከተልም ብሩኽ ውሁድ (ሲሊሲክ) ገሞራ-ትፍ የቅልጥአለት ፍሰት ውጤቶችን በመፍጠር ያበቃል። ልክ እንደ ጭልም ውሁድ (ባዛልቲክ) የቅልጥአለት ፍርክሶች፣ የሆፊ ሾጣጣ ኮረብቶችም እንዲሁ በገሞራ-ትፍ ፍሰት የተፈጠሩትን መደርመስ ሊደርስባቸው ይችላል። በቅርብ ጊዜ ከመውጫው በርቀት (distal) የተከማቹ የቅልጥአለት ፍርክሶች ምርምሮች ጎንለጎን እንደዚህ አይነት ፍንዳታዎች ቢያንስ በአሉቶ፤ ልኬታቸው ከሃይለኛ-ስትሮምቦሊያን እስከ ንዑስ-ፕሊኒያን ባለው መሀል ሆነው በ ጥንካሬ እና በመጠን ይለያያሉ፤ እያንዳንዳቸውም በሚያስደንቅ ሁኔታ ተመሳሳይ የሆነ ቅደም ተከተል የፍንዳታ ሂደቶች ይከተላሉ የሚል ሀሳብ እናቀርባለን።ቁልፍ-ቃላት: የሆፊ ሾጣጣ ኮረብቶች ፣ ሀይለኛ ፍንዳታ ፣ የቅልጥአለት ፍርክሶች ዴንሲቲ ማዕበል፣ የአሉቶ እሳተ ገሞራ ፣ ኢትዮጵያ

Keywords: Pumice cone; Explosive eruption; Pyroclastic density current; Aluto volcano; Ethiopia.

1 Introduction

Pumice cones are primary volcanic landforms comprising deposits of pumiceous tephra that rapidly thin away from the vent; developing a cone or rampart. They are found at silicic volcanoes worldwide, and have often been associated with peralkaline rhyolite compositions [Houghton et al. 1985; Mahood and Hildreth 1986; Orsi et al. 1989]. The eruption and construction of a pumice cone has never been observed and recorded; as such, the dynamics and styles of such eruption are largely unknown. Studies focusing on the eruption style and dynamics of pumice cone eruptions are relatively rare, and so far limited to Pantelleria, Italy [Orsi et al. 1989; Hughes et al. 2017], Tuhua (Mayor Island), New Zealand [Houghton et al. 1985], Lipari, Italy [Davì et al. 2011], Puʻu Waʻawaʻa, Hawaii, USA [Shea et al. 2017], Montaña Blanca, Tenerife, Spain [Ablay et al. 1995], Newberry caldera, USA [Higgins 1969; 1973], Payún Matrú caldera, Argentina [Hernando et al. 2019], and recent work in Ethiopia [Hutchison et al. 2016b; Fontijn et al. 2018; McNamara et al. 2018; Clarke et al. 2019]. Peralkaline rhyolite pumice cones on Tuhua have been interpreted to erupt in a Strombolian fashion; namely that pumice cones are formed by the accumulation of pumice around the vent by ballistic deposition during relatively low-magnitude and low-intensity eruptions [Houghton et al. 1985]. By contrast, the rhyolitic Lami succession pumice cone on Lipari, and the central pumice cone at Newberry are thought to have formed

* ase-benjamin.clarke@ntu.edu.sg

during more explosive pyroclastic eruptions depositing relatively widespread tephra fall deposits, and in the case of Lipari, generating pyroclastic density currents (PDCs) [Higgins 1969; Davì et al. 2011]. Similarly, recent work in the Main Ethiopian Rift (MER), where pumice cones comprise the most recent volcanism at many peralkaline rhyolite calderas [Hutchison et al. 2016b; Fontijn et al. 2018; McNamara et al. 2018; Clarke et al. 2019], has indicated that eruptions are intense (vulcanian to sub-Plinian) and unsteady. These differences in interpretation demonstrate that the intensity, magnitude, and processes that occur during pumice cone eruptions are somewhat ambiguous and perhaps diverse. This presents a challenge when assessing the hazard and risk around the many volcanoes worldwide which produce pumice cones. Here, we investigate the deposits of numerous pumice cone eruptions from Aluto; a populated caldera volcano in the Main Ethiopian Rift. By investigating the proximal and medial deposits, in conjunction with existing work on distal tephra fall deposits from Aluto, we attempt to understand the nature of these eruptions in terms of their eruptive and depositional processes. The ultimate aim is to characterise pumice cone eruptions more generally, and to inform volcanic hazard assessments for pumice cone-producing volcanoes.

1.1 Aluto volcano

Aluto volcano is situated in the central section of the Main Ethiopian Rift, between Lake Ziway to the north and Lake Langano to the south (Figure 1). The towns of Ziway (Batu), Adami Tulu, and Bulbulla lie ~7–10 km from Aluto's western flank, but many smaller settlements are scattered across Aluto's edifice and surrounding plains, including a school and a geothermal power facility within the margins of the caldera. The Aluto volcanic complex evolved as a trachytic shield volcano, and at around 310 ka, it underwent one or two major rhyolitic eruptive episodes that developed a 42 km^2 elliptical caldera [Hutchison et al. 2016b]. Post-caldera eruptive activity since at least 60 ka has been dominated by the development of numerous overlapping peralkaline rhyolite pumice cones which, along with obsidian lava flows and PDC deposits, obscure much of the older edifice [Hutchison et al. 2016b; Fontijn et al. 2018; Clarke et al. 2019; Clarke 2020; Clarke et al. 2020; Tierz et al. 2020]. These pumice cones are spatially clustered [Clarke et al. 2020]. The patterns of clustering, and elongation orientations of their craters, indicate the presence of two underlying fault sets at Aluto (NE/SW and NNE/SSW) and an elliptical caldera fault [Hutchison et al. 2015]. These structures have provided the pathways for magma and hydrothermal fluids since caldera collapse [Hutchison et al. 2015; Hunt et al. 2017]. The youngest dated pumice cone at Aluto is around 400 years old (0.4 ± 0.05 cal. ka BP) [Hutchison et al. 2016b], but material for radiometric dating is sparse [Fontijn et al. 2018] meaning that Aluto's chronostratigraphy [alongside many other volcanoes in the Main Ethiopian Rift] is relatively poorly constrained. The distal deposits of Aluto's Holocene post-caldera activity can be found in the lacustrine tephra record. The Central Main Ethiopian Rift (CMER) currently hosts four separate major lakes (Figure 1): Ziway, Langano, Abijata, and Shala, which have a complex history of water-level fluctuation, interconnection, and separation since the early Pleistocene [Benvenuti et al. 2002; 2009]. These basins have collected the distal tephra fallout of several CMER volcanoes, including Aluto; providing ages for a selection of Holocene eruptions [Fontijn et al. 2018; McNamara et al. 2018]. From the Langano and Abijata lake cores, McNamara et al. [2018] found that the time-averaged recurrence rate of eruptions from Aluto (that are sufficiently intense to deposit tephras in the surrounding lakes) is around once every 250 years. However, over the last 12 ka, these events are concentrated in temporal clusters (at 3, 6.5, and 11 ka), where eruptions occur roughly once every 100 years [McNamara et al. 2018]. Based on distance-thickness relationships of lake tephras, McNamara et al. [2018] also tentatively describe the Aluto eruptions to range in intensity, magnitude, and style from vulcanian to sub-Plinian [McNamara et al. 2018].

2 Methods

2.1 Fieldwork and stratigraphic framework

Fieldwork was conducted over two field seasons at Aluto in 2015 and 2017, totalling seven weeks. Sites were chosen according to exposure, to ensure coverage of the full range of pumice cone morphologies visible by remote sensing, and to cover a wide geographic range around Aluto. Sites were logged, and individual stratigraphic units were described and traced laterally. Stratigraphically adjacent eruption units are distinguished by the presence of intermediate palaeosols. The rate of historical and modern soil formation in the Main Ethiopian Rift, as in many locations globally, is poorly constrained. Consequently, it is possible temporally close eruptions may not be distinguishable. However, where a palaeosol does not exist, and where there is no further evidence of a time gap, it is simplest to assume pyroclastic units are associated with the same eruption. We employ the lithofacies scheme for describing pyroclastic deposits recommended by Branney and Kokelaar [2002], a relevant subset of which is summarised in Table 1. Following Branney and Kokelaar [2002], we also use the term 'ignimbrite' to refer to any deposit from a PDC, irrespective of a particular deposit volume or PDC generation mechanism. Pyroclastic units from pumice cones at Aluto often have a small lateral distribution (100s of meters to a few kilometers), and the geochemistry of peralkaline rhyolite glasses from different eruptions is remarkably homogeneous and often indistinguishable [Fontijn et al. 2018; McNamara et al. 2018]. This permits only localised stratigraphies; where lateral documentation of pyroclastic units is limited to physical tracing, and tracing of geomorphological features visible in the available 2 m resolution LiDAR topographic data set of Aluto [Hutchison et al. 2014]. This precludes most correlation across the edifice as a whole, and between terrestrial tephras and lake tephras, for which there is a better-developed chronostratigraphic framework [Fontijn et al. 2018; McNamara et al. 2018]. For terrestrial deposits in the arid MER, there is a paucity of material suitable for ^{14}C dating [Fontijn et al. 2018], though there are some Ar-Ar dates from K-feldspar bearing pumices and lavas at Aluto [Hutchison et al. 2016a]. Collectively, these provide a temporal bracket for the post-caldera eruption de-

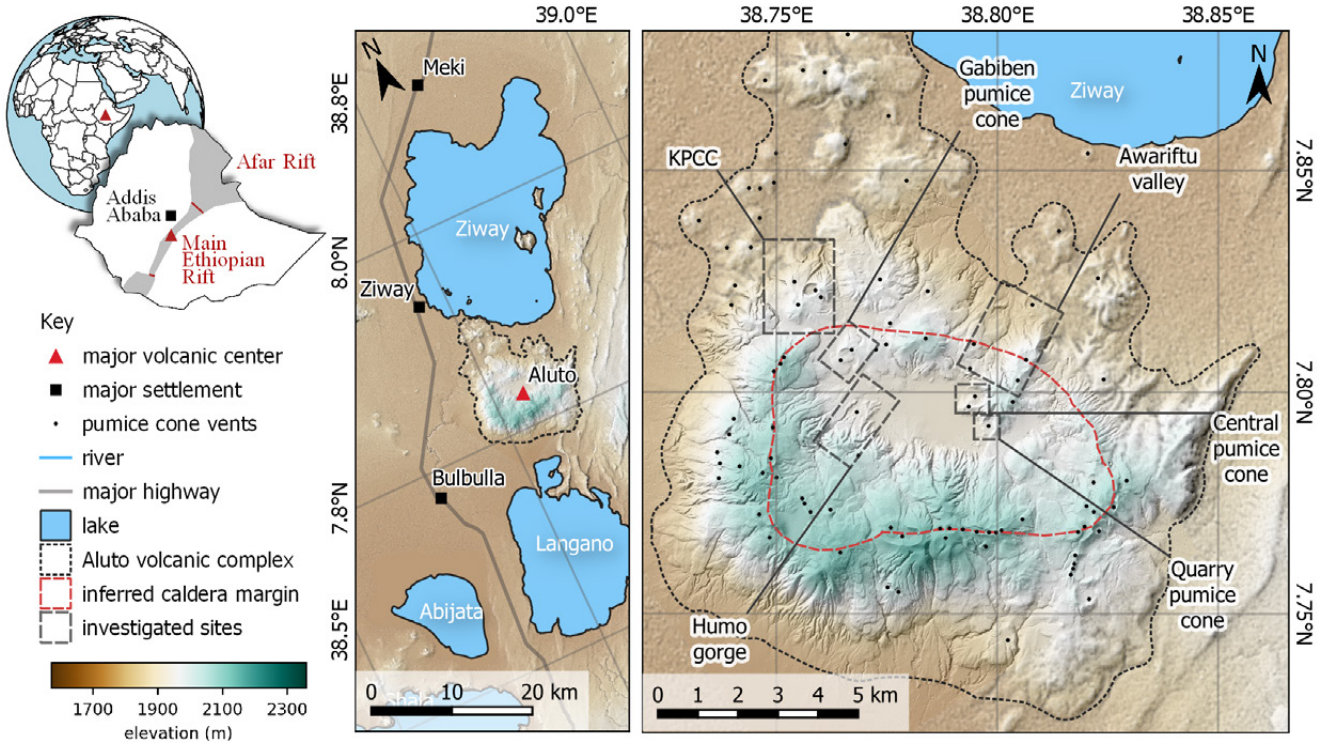

Figure 1: Overview of Aluto volcano, showing the regional and local context [after, Clarke et al. 2020; Tierz et al. 2020]. This includes the field sites investigated here, pumice cone vents at the surface identified around Aluto, and the inferred (and partially exposed) caldera ring fault from [Hutchison et al. 2016b]. Aluto topography is a 2m LiDAR dataset [Hutchison et al. 2014], regional topography is 1 arc second (approx. 30 m) SRTM [NASA 2014].

posits at Aluto of between 306 ± 12 ka (Ar-Ar) and 0.4 ± 0.05 ka (^{14}C) [Hutchison et al. 2016a]. Where more precise age constraints for particular deposits or sequences are available, they are provided in this work. As we present here, the history of post-caldera volcanism at Aluto is one of discrete eruption centres that spatially overlap to a greater or lesser extent. Due to these constraints, we do not attempt to develop a comprehensive chronostratigraphy of post-caldera volcanism at Aluto. However, by exploring the nature of eruptions at Aluto in a series of eruption case studies, and comparing them with findings from lake-tephra investigations, we attempt to evaluate the nature of pumice-cone-forming eruptions at Aluto.

2.2 Granulometry

Bulk samples of loose pyroclastic deposits, free of soil and surface-wash were sampled, and ensuring a representative mass was sampled (so that no single pyroclast exceeded 5 wt.% of the total sample mass [Mosley and Tindale 1985]). Deposits were first sieved in the field for fractions coarser than −2 ϕ (> 4 mm) at 1 ϕ intervals, and sorted by their componentry (pumice, obsidian, volcanic lithic, sedimentary lithic). Pumice was defined as pale, qualitatively low-density and microvesicular material. The remaining fine fraction was coned and quartered one or two times for laboratory sieving. The fine fractions were dried at 100 °C for at least 24 hours, and hand-sieved at 1 ϕ increments up to 5 ϕ (> 0.031 mm). The pumice to lithic ratio was quantified for size fractions coarser than 1 ϕ (> 0.5 mm) by complete manual assessment of coned-and-quartered sub-samples. The mass of the remaining fines (> 5 ϕ, < 0.031 mm) was taken for each sample, and in all cases comprised < 5 % of the total sample mass. Granulometry statistics (Inman parameters [Inman 1952]) were calculated from empirical cumulative grain size distributions using a custom `Python` script without normalisation to 100 wt.%. As Inman parameters only assess the central (16th–84th) cumulative percentiles, the open-ended fine-tail of the distribution does not influence comparative grain size statistics. Granulometry and componentry data can be found in Supplementary Material 1.

Table 1: A selected overview of the pyroclastic lithofacies scheme of Branney and Kokelaar [2002] used throughout this work, including the facies abbreviations used in the text.

Abbreviation	Lithofacies
Prefix	
m	massive
s	stratified
xs	cross stratified
dxs	diffusely cross stratified
ds	diffusely stratified
Suffix	
T	tuff (clasts <2mm)
LT	lapilli tuff (2 mm >clasts <64 mm)
BT	block/bomb tuff (clasts >64 mm)
Br	breccia

3 Results

3.1 Facies descriptions and interpretations

Pumice cones at Aluto display a variety of pyroclastic deposits which can be broadly categorised into the following facies. Here we describe and interpret these facies, and sets of facies, which form the basis of eruption stratigraphies explored later.

3.1.1 *Cone-forming massive pumice breccias: mLBr*

Description Common to every pumice cone investigated at Aluto is the cone-forming, massive pumice breccia facies (Figure 2A). They form shallow cones with outer slopes below the angle of repose. These are characteristically coarse ($Md_\phi \approx -1.5$ to -5), very well to poorly sorted ($\sigma_\phi \approx 1$–3), clast-supported, open-work angular lapilli to block breccias (Figure 3). The primary juvenile phase is pumice, which is sometimes in a 'jigsaw' form (i.e. fractured, but complete clasts) [e.g. Wilson and Hildreth 1998], forming approximately <10 vol.% of the deposits. Deposits sometimes contain juvenile flight quenched and deposit quenched pumiceous achneliths (FQAs and DQAs) [*sensu* Clarke et al. 2019]), which are fluidal pyroclasts with a thin skin and a pumiceous interior that variously indicate post-fragmentation (FQA and DQA) and post-deposition (DQA) ductile deformation above the glass transition [Clarke et al. 2019]. As the proportion of pumiceous achneliths increases, the deposit may become incipiently welded, but in general, welding is absent in these deposits. Deposits sometimes contain rare obsidian breadcrust bombs and angular, dense, coarse-ash to block-sized glassy obsidian fragments. It is uncertain whether they are juvenile to the deposit-forming eruption, or are an accidental component. Lithics (excluding dense glassy obsidian) generally form a small volume fraction of the deposit (absent to <10 vol.%), but where they are present comprise green welded ignimbrite, dense undifferentiated oxidised lavas, and fine grained sedimentary rocks. Apart from occasional outsized blocks, dense components are generally smaller than adjacent low-density pumice clasts. Systematic vertical and lateral grading patterns are common in these deposits. Laterally, grain size decreases monotonically from the inferred vent. Vertically, grading can be continuous and gradational (normal, inverse, or combinations), or discontinuous over a short length-scale (cm to meters). Commonly, grain size decreases towards the top of the deposit. In some cases, they develop diffuse slope-parallel bedding structures with a gradational transition into the lensoid bedded inversely graded pumice breccia facies (bLBr, described later). The deposits are coniform, often forming the main body of pumice cones. Typically, maximum deposit thicknesses are 10s of meters, but some cones are tall (<150 m) and comprise only this facies. In some cases, this facies grades laterally into widespread sheet-like massive lapilli (mL) or massive tuff (mT) facies.

Interpretation The angularity, clast support, presence of 'jigsaw' pumices, and the hydraulic equivalence of clasts [Burgisser and Gardner 2006] within these deposits, as well as their draping of underlying topography, indicates that they are fall deposits. While jigsaw-fit breccias are characteristic of block facies in debris avalanche deposits, where tessellating clast fragments remain adjacent despite flowing considerable distances by acoustic fluidisation [Melosh 1987; Glicken 1991], jigsaw pumices are a distinct phenomenon. They are small individual clasts, rather than larger deposit domains, do not display fluidal domain margins, and the overall deposit architecture is inconsistent with debris avalanches. Instead, they indicate a lack of transport after they have fractured on impact. mLBr is very similar to early facies of shallow scoria cones globally [e.g. Valentine et al. 2007], and massive facies within some maar deposits (e.g. Figure 2B, Meerfeld maar - Eifel), which develop around eruption vents by a multitude of concurrent fall-processes [McGetchin et al. 1974; Riedel et al. 2003; Houghton et al. 2004]. Where present at Aluto, low-density (0.2–0.8 g cm^{-3}), lapilli-sized DQAs show that at least a subset of their clasts are deposited from the edge of an eruption column [Clarke et al. 2019]. However, at proximal locations, it is likely that outsized blocks and coarse breadcrust bombs represent a ballistic component. The lateral-grading of some of these deposits to widespread sheet-like fall deposits implies that these breccias contain tephra that has fallen from an umbrella cloud. This diversity of emplacement mechanisms close to the vent is likely to be the origin of their often relatively poor sorting, atypical of medial to distal tephra falls deposited from an umbrella cloud only [e.g. Walker 1971]. Highly variable, and often poor sorting has been recognised more generally in proximal cone or rampart-building fall deposits from intense eruptions [e.g. Walker et al. 1984; Hildreth and Drake 1992; Fierstein et al. 1997; Houghton et al. 2004], and poorer sorting is expected closer to volcanic vents in general [Sparks et al. 1992]. We cannot rule-out hydrovolcanic interactions during pumice cone eruptions at Aluto, indeed some mLBrs resemble coarse grained, hydrovolcanic maar deposits (Figure 2A, 2B), and the presence of lahar deposits (see section on volcaniclastic facies) implies a humid environment. However, there is little positive evidence for any prolonged phreatomagmatic behaviour, such as rhythmic fine bedding/lamination, slumping, induration, abundant ash aggregates, dense juvenile population, or the generally (though not ubiquitously [e.g. Pedrazzi et al. 2014]) fine grained nature typical of near-vent phreatomagmatic deposits [e.g. Self and Sparks 1978; Kokelaar 1983; White and Valentine 2016]. Vertical grading patterns at a given locality in fall deposits are a function of total grain size distribution, eruption intensity and wind direction(s) [Pyle 1989]. Without robust isopachs and isopleths it is impossible to disentangle these features, but the frequent reduction in average grain size towards the top of these units, followed stratigraphically by mLTs (deposited by PDCs, discussed later), implies that a waning eruption intensity was common towards the end of fall deposition.

3.1.2 *Lensoid bedded, inversely graded pumice breccias: bLBr*

Description In many pumice cones at Aluto, where they are deposited on a steep slope or develop a steeper and taller cone morphology, massive pumice breccias transform vertically into lensoid bedded inversely graded pumice breccias (bLBr) (Figure 2C). These breccias are angular, clast-supported

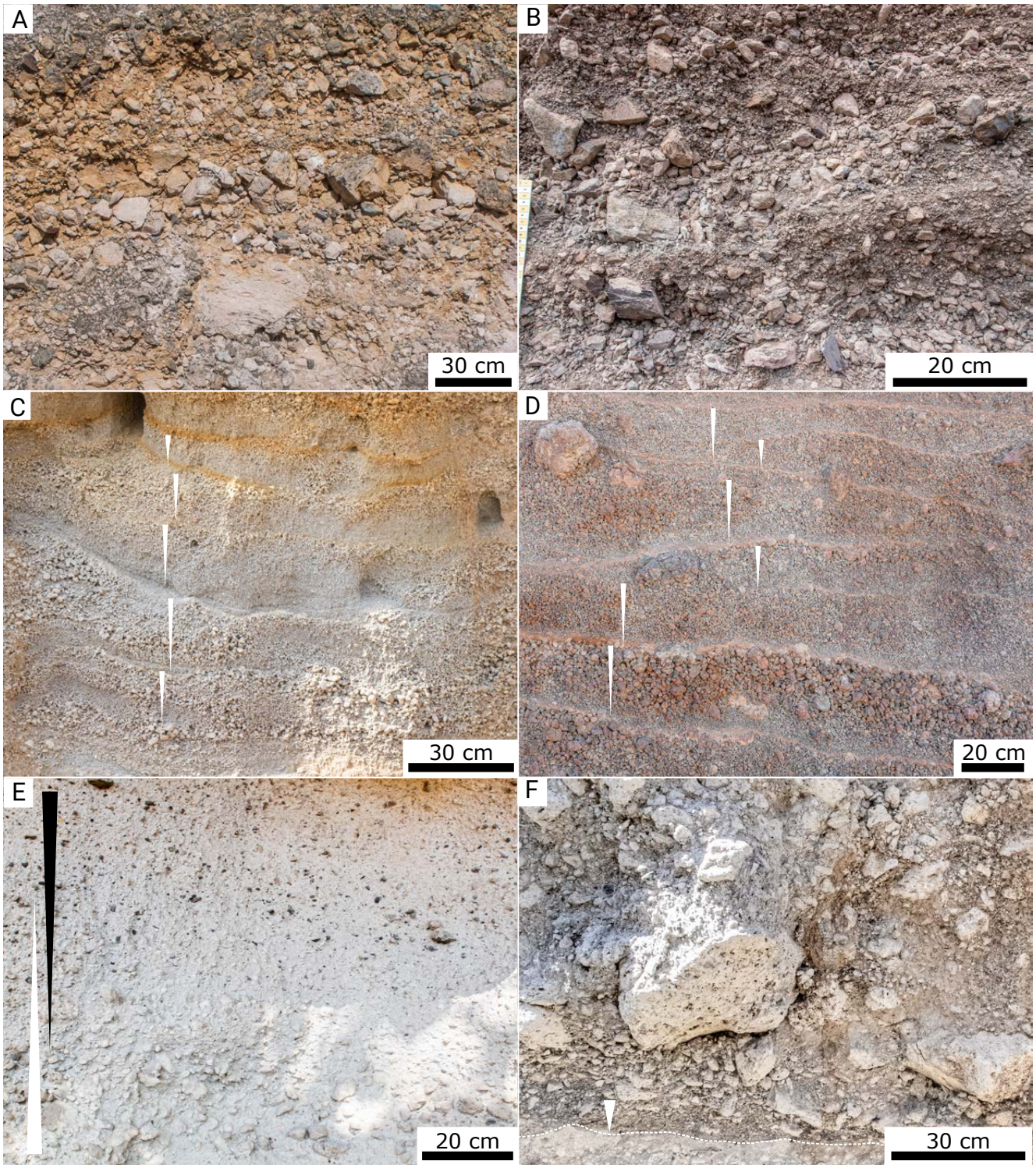

Figure 2: The most common primary pyroclastic facies at Aluto pumice cones, and comparisons with cone-building facies in similar volcanic systems. [A–B] massive, clast-supported, open-work angular juvenile-rich lapilli to block breccias at [A] Quarry pumice cone, Aluto, and [B] Meerfelder maar, Eifel (Germany). [C–D] Lensoid bedded, inversely graded pumice lapilli breccias at [C] Aluto, and [D] Megalo Vuono scoria cone, Santorini. [E] Matrix-supported massive lapilli tuff showing antithetical grading of pumice (white triangle) and lithics (black triangle) (unit H7, Humo 1 eruption) Aluto. Here indicating deposition from a waxing density current. [F] Matrix-poor massive lapilli/block tuff with a inversely graded fine grained base and rounded pumices (unit A12, Awariftu 2 eruption) Aluto.

and open-work. They are characterised by their steep bedding surfaces which are generally close to angles of repose (≈ 25–30°) that dip away from the cone center, inverse grading normal to bedding, and discontinuous lensoid bedding structure. Lensoid beds are typically on the scale of cm to 10s of cm vertically, with a lateral span of 10s of cm to meters. 'Jigsaw' pumices are absent, and the deposits are qualitatively less rich in dense components than underlying massive pumice breccia facies.

Interpretation An identical facies to bLBr is commonly observed in the upper stratigraphy of basaltic scoria cones (Figure 2C versus 2D) where the repose angle of the constituent material is reached, leading to small grain flows down the cone slopes [e.g. McGetchin et al. 1974; Sohn and Chough 1993; Riedel et al. 2003]. This process sorts tephra by size and density, creating the characteristic inverse grading. Denser lithic material also flows further downslope, therefore depleting the upper deposits in lithic material [Sohn and Chough 1993]. This facies is not always restricted to the later stages of cone growth, for example if cones accumulate on surfaces close to the repose angle. This facies indicates that pumice cones grow in a very similar fashion to most basaltic scoria cones: by lateral grainflow with simulataneous column-edge and ballistic deposition [Riedel et al. 2003; Valentine et al. 2005; Martin and Németh 2006; Pioli et al. 2008].

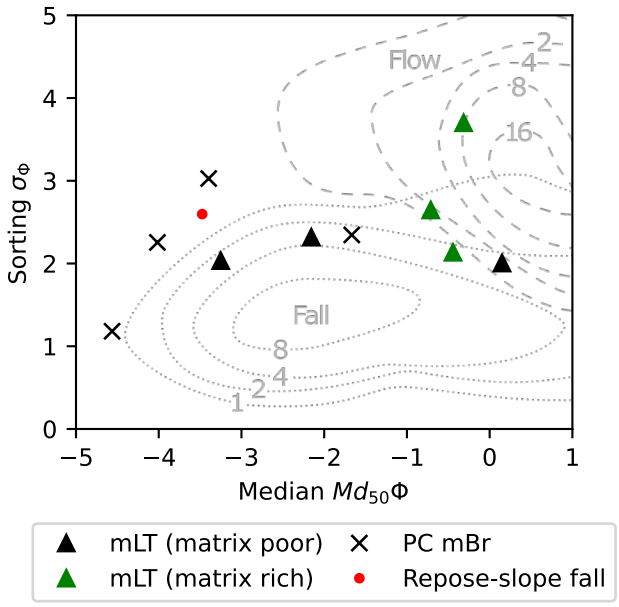

Figure 3: Median-grain size versus sorting of pyroclastic pumice cone-forming deposits from Aluto: massive lapilli/block breccias (mLBr), lensoid bedded lapilli breccia (bLBr), matrix-rich and matrix-poor massive lapilli tuffs (mLTs). Including fall/flow fields established by Walker [1971]. mLBrs and bLBrs are characteristically coarse, and more poorly sorted than common pyroclastic fall deposits. Matrix poor mLTs are coarser than typical mLTs due to their lack of matrix. Sorting is calculated as the Inman sorting parameter [Inman 1952].

3.1.3 *Massive to parallel-stratified tuff and lapilli*

Description Much of the rift floor around Aluto comprises massive tuff and massive lapilli (mT, mL) and parallel stratified tuff and bedded lapilli (sT, bL). These facies are occasionally found within proximal pumice cone stratigraphies at Aluto. They are clast-supported, juvenile pumice/ash rich deposits, that may also contain various proportions of angular dense lithic fragments, that tend to be finer grained than the lower density pumice component. mL facies are well to very-well sorted open-work angular pumice breccias that mantle topography. They may also display planar bedding, where they are described as bL. These facies are gradational into mT and sT according to grain size. Grain size variations are laterally systematic, and sometimes exhibit normal or reverse vertical grading. Such deposits are often sheet like, showing little thickness variation over the exposure-scale, but have occasionally been found to thicken and grade into cone-forming mLBr over a scale of 100s of meters. As with many facies at Aluto, transitional diffusely bedded or stratified facies (dbL, dbT) have also been identified.

Interpretation In most cases, the well-sorted, angular pumices, and mantling of topography indicates that these facies are pyroclastic fall deposits derived from a plume. Where they are lapilli sized (mL, bL), and sheet-like in form, they are likely to have fallen from an umbrella cloud, centred on a comparatively proximal vent. Where they are ash sized (mT, sT) they may be more distal deposits of an umbrella cloud (from Aluto, or perhaps another nearby volcano), or co-ignimbrite fall deposits from Aluto. In such cases, contextual evidence (such as underlying ignimbrites) must be used to distinguish origin. The presence or absence of planar stratification is indicative of eruption column steadiness, and vertical grading indicates changes in eruption intensity, changes in wind direction during the eruption or changes in fragmentation efficiency at the vent (modifying the total grain size distribution) [Sparks et al. 1997; Bonadonna and Houghton 2005]. The mT facies may be pyroclastic fall or flow in origin, potentially representing the deposit of a steady ash fall, a concentrated but fine-grained PDC [Branney and Kokelaar 2002], or even a water-lain volcaniclastic deposit. Further evidence, such as lateral or vertical grading into other facies, diffuse cross stratification, evidence of water during deposition, presence of accretionary lapilli, and relationship to topography must be taken holistically to determine an origin.

3.1.4 *Massive lapilli tuff (matrix-supported)*

Description Massive lapilli tuffs at Aluto are most commonly matrix-supported (Figure 2E). These are poorly to very poorly sorted ($\sigma_\Phi \approx 2$–4) mLTs (and mBTs) with sub-rounded to well-rounded pumices, a variety of angular lithic components (obsidian, and older pyroclastic and epiclastic rocks), set in an ashy matrix. Pumice and lithic populations are commonly, but not always, antithetically graded (e.g. Figure 2E). Some mLTs at Aluto display a thin (<10 cm), inversely graded fine-grained base. Neither elutriation pipes nor clast imbrication have been observed in mLTs at Aluto. Matrix-supported mLTs are most often found in medial and distal

drainages/gorges around the volcano. Where deposits are laterally confined, deposits may reach over 20 m thick, but are more typically on a scale of 10s of cm to meters. The most distal mLTs have been found 5 km from their inferred source, where they reach the edge of palaeolake Langano (thus representing a minimum distance). So far, all mLTs from post-caldera eruptions that have been found at Aluto are loosely consolidated or lightly indurated; welding is entirely absent.

Interpretation The poor sorting, rounded pumices, topographic confinement, fine-grained bases, antithetical grading of pumice, and lithic populations indicate these are the deposits of pyroclastic density currents [Branney and Kokelaar 2002]. Massive lapilli tuffs are typically ascribed to a granular fluid–based PDCs, where clast concentration in the lower flow boundary zone is high, suppressing turbulence and producing massive deposits, or where the lower flow boundary zone is dominated by fluid escape [Sparks 1976; Branney and Kokelaar 2002; Smith et al. 2020]. The apparent lack of imbrication in these mLTs implies that shear is relatively low, and so a fluid escape–dominated, rather than granular flow–dominated lower flow boundary zone is likely to be the typical dynamic mode for such PDCs at Aluto [Branney and Kokelaar 2002]. The lack of elutriation pipes, which are often found in systems with a fluid-escape dominated lower flow boundary zone, might indicate a generally low sedimentation rate [Branney and Kokelaar 2002]. Their close association with underlying fall deposits, the juvenile phase mostly comprising vesicular pumice, and the lack of evidence for steep sided lava domes, indicates that PDCs at Aluto are generated by column-collapse.

3.1.5 *Massive lapilli tuff (matrix-poor)*

Description Some proximal mLTs at Aluto are matrix-poor (Figure 2F), such that they are, or approach, a clast-supported structure. They contain sub-rounded to well-rounded pumices. Like some matrix-supported examples, they also display a fine-grained base, contain an ashy matrix, are poorly sorted, and thicken into topographic lows. These deposits are better sorted ($\sigma_\phi \approx 2$) and often coarser than matrix-supported mLTs owing to their paucity of matrix (Figure 3). These deposits are often lithic-rich, where dense and lithic components exceed the volume fraction of low density juvenile pumices. At Aluto, matrix-poor mLTs are generally found on proximal cone slopes, and thicken into drainages where they sometimes transform into matrix-rich mLTs.

Interpretation Similar to matrix-supported mLTs, matrix-poor mLTs at Aluto possess typical features of flow deposits, apart from their (near) clast-supported structure. They lack the 'block facies' generally associated with debris-avalanche deposits [Glicken 1991], and sometimes grade into matrix-supported mLTs. The paucity of matrix, as well as the coarseness and lack of elutriation pipes in some of these deposits is similar to 'hybrid' proximal deposits described at a number of plinian vents [Dowey and Williams 2022]. However, at Aluto these grade laterally and vertically into matrix-supported mLTs, rather than fall deposits as described for 'hybrid' deposits. In other volcanic systems, lithic-rich and fines-poor breccias have been recognised close to their source vent, and are thought to result from the compression of gas and expulsion of low-density and fine material at the 'impact site' of a collapsing eruption column [Valentine and Sweeney 2018]. This is effectively a broad scale elutriation process, and may explain the lack of discrete pipes, and the common enrichment of dense lithic clasts in the clast-supported mLTs. Similar matrix-poor proximal ignimbrites have been recognised at Novarupta [facies C_d Houghton et al. 2004]. At Novarupta, the lack of matrix is thought to reflect either limited comminution of pumice over a short flow distance, or that the PDCs are derived from gravitationally unstable, unconsolidated fall deposits. Either situation is plausible at proximal locations on steep-sided pumice cones. However, at Aluto, the pumices are sub- to well-rounded, indicating that significant comminution has already taken place, which is hard to reconcile with the remobilisation of recently deposited angular pumice fall deposits. We therefore attribute proximal matrix-poor mLTs to a proximal column-collapse ignimbrite facies, where fines have been expelled due to high fluid pressures in an 'impact zone' of a collapsing column. At greater flow distances, increased comminution of pumice in these density currents generates more fine ash forming the matrix of medial to distal matrix-supported mLTs.

3.1.6 *Cross stratified tuffs and cross stratified lapilli tuffs*

Description Pumice cones at Aluto occasionally exhibit cross stratified tuffs (xsT) and cross stratified lapilli tuffs (xsLT). These are finer grained and better sorted than mLTs, possess low-angle forsets often marked by discontinuous strings of coarse ash and rounded pumice lapilli. Only one such deposit has found to contain accretionary lapilli, and are rare in this deposit, with only a few individual aggregates visible in meters of lateral exposure. The main juvenile component is fine ash, and small pumice lapilli. These deposits are generally lithic poor, but contain medium- to coarse ash–sized angular fragments of glassy obsidian. Such deposits often pinch and swell in thickness, where the maximum thickness observed is 1.5 m. Cross stratified tuffs often gradationally transform into or from matrix-supported mLT. Occasionally, an intermediate diffusely bedded or diffusely cross stratified lapilli tuff (dbLT/dxsLT) facies is found, with poorly developed stratification or cross stratification.

Interpretation The gradational transition between xsTs/xsLTs and mLTs, as well as rounded pumices, poor-sorting (compared to fall deposits), topographic pinching and swelling, and cross bedding indicate they are flow deposits. Cross bedding and stringers of larger clasts imply a turbulent, tractional-dominated lower flow boundary zone, considered to be typical of PDCs with lower particle concentrations and higher shear rates [Branney and Kokelaar 2002; Smith et al. 2020]. Their gradational relationship with mLTs indicates fluctuations in density-current particle concentration in space and time. The rare presence of accretionary lapilli does not alone indicate a hydrovolcanic origin, particularly considering their paucity. dbLTs and dxsLTs indicate intermediate

conditions of particle concentration within the lower flow boundary zone between mLT and fully developed xsT/xsLT.

3.1.7 *Silicic lavas*

Description Silicic lavas are commonly the final product of pumice cone eruptions at Aluto, and are a conspicuous feature of Aluto's landscape. They occur at six out of the nine pumice cones investigated here, but many more lavas can be observed in satellite imagery and in the DSM of Hutchison et al. [2014]. They range in form from coulees (showing little asymmetry and down-slope movement), to elongate multilobed lava flows with a maximum flow distance of 2.3 km from source. Surface folds (ogives) are present on all silicic flows at Aluto. Where lower contacts are exposed, they are sharp, onlap underlying stratigraphy, and entrain local underlying clasts within the bottom meter, locally with an autobreccia. Flow fronts are often steep (near vertical) and comprise blocky rubble. The flows comprise discontinuous and somewhat irregular domains of microvesicular lava and glassy obsidian. Obsidian lavas are occasionally flow banded. Petrographically, silicic lavas at Aluto are generally crystal rich, containing quartz, K-feldspar, aegirine, and aenigmatite in a glassy groundmass. Most crystals comprise a core of K-feldspar with a rim of granophyric quartz and K-feldspar that overgrows nearby phenocrysts of aegirine and aenigmatite. Lavas from Aluto pumice cones are strongly peralkaline rhyolites on a whole-rock geochemical basis [*sensu* Mahood 1984] [Hutchison et al. 2016b].

Interpretation Globally, silicic lavas are typically emplaced during the later stages of silicic eruptions, and sometimes simultaneously with explosive eruptive activity [Schipper et al. 2013; Castro et al. 2014]. Recent work suggests such lavas form by the viscous sintering of explosively fragmented pyroclasts that block the conduit, and flow from the vent driven by pressure from the ash-gas mixture below [Wadsworth et al. 2020; Foster et al. 2024]. Investigations of ogives on similar Ethiopian peralkaline rhyolite lavas at Corbetti and Fantale volcanoes indicate emplacement viscosities similar to calc-alkaline rhyolites [Hunt et al. 2019]. Granophyric crystals at Aluto have been previously interpreted as xenocrysts of undercooled granitic wall-rock [Lowenstern et al. 1997; Hutchison et al. 2016b]. While this work primarily focusses on the explosive pyroclastic processes involved in Aluto pumice cone eruptions, the occurrence of silicic lavas at the end of pumice cone eruptions is consistent with a late-stage fragmentation, sintering and flow from the vent.

3.1.8 *Debris flow, hyperconcentrated flow, and normal streamflow facies*

Description Volcaniclastic deposits are found within Aluto pumice cone stratigraphies and modern drainages around the volcano. The distinction of volcaniclastic from pyroclastic deposits can be challenging, and is often a holistic interpretation based on sedimentological and broader contextual evidence [Cowlyn et al. 2020]. Central to the distinction of volcaniclastic deposits is evidence of aqueous deposition. Here, we use several (variously concurrent) features to distinguish this: the presence of bubbles in matrix, load and flame structures, well developed cross bedding or climbing ripples, and clasts that are strongly density-segregated into laminations. Such deposits may also appear anomalously muddy, indurated, or contain an anomalous componentry to stratigraphically adjacent deposits. They may also fill rills, or V- or box-shaped gullies (that are typical of water-induced incision [Collins and Dunne 1986]) rather than wider u-shaped gullies that are associated with PDCs [Kieffer et al. 2021]. We distinguish three main volcaniclastic facies at Aluto: debris flow facies, hyperconcentrated flow facies and normal streamflow facies. Debris flow facies at Aluto are usually mLTs; very poorly sorted matrix-supported massive deposits, but tend to have a higher proportion of clay-sized material than pyroclastic mLTs and are commonly normally graded, and sometimes contain bubbles in their matrix. In some cases, they may instead be better sorted (lacking a the coarse-tail of an mLT) and massive. Hyperconcentrated flow deposits share many of the same characteristics, but are finer grained with occasional pumice lapilli sized clasts, are usually better sorted than debris flow deposits, often massive or parallel laminated. Dewatering structures, commonly associated with hyperconcentrated flow and debris flow deposits [Druitt 1995], have not been observed at Aluto. Normal streamflow deposits are sands and conglomerates that may display the range of common fluvial sedimentary structures formed through turbulent suspension and tractional flow processes, such as cross bedding, climbing ripples and low angle cross bedding [e.g. Smith 2000]. They are usually better sorted than pyroclastic flow facies, and can be distinguished by their clast-support and lack of fine ash. At Aluto all these facies are channel-filling, but hyperconcentrated flow deposits are also found as an overbank-facies associated with channel filling debris flow deposits [e.g. Vallance and Iverson 2015].

Interpretation Debris flow, hyperconcentrated flow and normal streamflow deposits are the product of sediment-laden aqueous flows, with a spectrum of high to low volumetric ratios of sediment to water respectively [Pierson and Scott 1985; Pierson and Costa 1987]. The presence of bubbles in the matrix of some deposits at Aluto is not a definitive character of volcaniclastic sediments, as they have been described in 'vesiculated tuffs' associated with wet PDCs from Surtseyan style eruptions [Lorenz 1974]. Bubbles instead indicate the presence of water on deposition. The presence of volcaniclastic deposits at Aluto is indicative of a humid environment and the re-mobilisation of loose pyroclastic material during and after eruptions. Volcaniclastic facies that fill rills on cone-slopes represent incision and re-mobilistation of loose tephra by rainfall, with high rates of erosion enabling sufficiently high sediment to water ratio to suppress turbulence during flow [Pierson and Costa 1987; Vallance and Iverson 2015]. Larger volume, gully-filling volcaniclastic deposits that tend to occur in larger drainages on Aluto's outer flanks also represent the aqueous remobilisation of tephra sourced from a larger catchment area. Where present, normal streamflow facies are found alone or above hyperconcentrated flow deposits, where they represent flows with more dilute sediment concentrations at waning stages of erosion and flow, or where erosion

rates were insufficient to generate more sediment rich flows. The source of water is likely to be rainfall over a caldera-scale catchment during eruption or volcanically quiescent periods, but some authors have tentatively suggested the presence of a caldera lake at Aluto during particularly humid periods [Hutchison et al. 2016b].

3.2 Eruption case studies

A high-resolution topographic data set (2 m resolution LiDAR digital surface model—DSM) [Hutchison et al. 2014] has allowed 86 eruptive vents to be identified across Aluto's edifice. These are identified as craters set into a topographic high (a cone or rampart), often with a silicic lava dome, couleé, or flow emanating from the vent. Each of these structures is defined here as a pumice cone. Exposures of these pumice cone deposits were investigated across a series of sites around Aluto, each providing a record of one or more pumice-cone-forming eruptions. These sites are the Kertefa Pumice Cone Complex (KPCC), Humo Gorge, Awariftu valley, and the Quarry, Central, and Gabiben pumice cones (Figure 1). Eruption stratigraphies from of the sites are described and eruptions individually reconstructed in the following sections.

3.3 Kertefa Pumice Cone Complex

The Kertefa Pumice Cone Complex (KPCC), is a series of overlapping pumice cones and ramparts on the NW edge of Aluto's edifice (Figure 1). The main sites investigated here are Kertefa gorge and South Kertefa Wadi (Figure 4), which collectively comprise deposits of at least three eruptions from the KPCC. Near the top of the exposed succession is a tephra fall deposit from the 'Qup' eruption (as defined in Fontijn et al. [2018]), identified by its rhythmic planar bedding and known stratigraphic position and thickness in this region of Aluto [Fontijn et al. 2018]. Deposits directly below the 'Qup', which are correlated with lacustrine and terrestrial sections, are dated to 7.3 ka [McNamara et al., unpublished data, Fontijn et al. 2018]; indicating the deposits of the KPCC are older than this.

KPCC 1 eruption The oldest pyroclastic units from the KPCC identified at Kertefa gorge are a series of dm-scale matrix-poor massive lapilli tuffs (mLTs), the upper most of which (K7) is shown in Figure 5. An underlying palaeosol to these deposits is not exposed. Above these is a silicic lava flow (K8) capped by a thin palaeosol, representing the end of the eruption. The limited exposure makes finding the source of these units challenging, but the presence of PDCs and a silicic lava implies the source is nearby; and is possibly 'vent 1' of the KPCC (Figure 4), where the partial burial by the pumice rampart from the KPPC 2 eruption indicates it is one of the oldest structures exposed at the KPCC. Above the palaeosol is a 1 m thick normally graded, framework-supported lithic-poor mL, containing lapilli-sized pumices with smaller obsidian lithics (K9). The unit can be traced along the length of Kertefa gorge (~500 m) and displays little change in overall thickness. Upwards, it transforms into a thick, patchy palaeosol. This is interpreted as a soilified fall deposit from an unknown source, and the presence of a palaeosol above and below indicates it represents a distinct eruption.

KPCC 2: The Diima eruption The second KPCC eruption, the 'Diima' eruption, named after the characteristic pink pumice that forms the bulk of the Diima pumice cone and rampart (*Diima* means 'pink' in the Oromo language), is exposed in Kertefa gorge and South Kertefa Wadi; represented by units K10 to K12 (Figure 5A). The first Diima deposit is a mLBr (K10) which forms the bulk of the pumice cone and the N–S aligned rampart visible in Figure 4. The outer slopes of the rampart are shallow (3°), but steepen towards the vent (20°). The inner crater slope of the rampart reaches around 30–35°. K10 thickens proximally from the western end of Kertefa gorge (0.5 m thick), towards the edge of the vent 2 pumice rampart (40 m thick) to the East (Figure 5B). At proximal locations (log K_a, Figure 5A, 460 m from vent) pumices are block sized, but grade to lapilli >750 m from vent. Vertically, the deposit grades inversely then normally, which is also reflected in a colour change of pumices from grey, to yellow to pink and back again (Figure 5B, 5C). This colour change reflects pumice size, and so distally exhibits a grey-yellow-grey sequence, and at greater distances, only grey. The K10 mLBr is followed by K11: a mLT that transforms vertically and laterally into a finer grained dxsT. The boundary between the mLBr and mLT varies laterally from very sharp (Figure 5C), to gradational (Figure 5B). The lower boundary undulates, with the the mLT filling topographic lows in the slopes of the mLBr. Distally, at the western end of the gorge, the mLT becomes less massive, and displays discrete internal discontinous lobate bedding. Assuming down-slope flow, the 3D architecture of these deposits implies this ignimbrite was deposited on a northward dipping slope, and so is thought to originate from the southern end of the pumice rampart (vent 2). The final exposed product of the Diima eruption is a silicic lava flow (K12), emanating from a small prominence (vent 4) at the southern end of the pumice rampart. The base of the silicic lava is auto-brecciated, and contains entrained and sometimes deformed characteristically pink pumices from unit K10. With height, the lava becomes dense and glassy, with occasional discontinuous microvesicular domains. At locations where the lava did not reach (SK_a, K_c), a palaeosol separates the K11 mLTs and dxsTs from those of the following KPCC eruption. The K10 mLBr represents a deposition from a steady pyroclastic eruption column. The grading of this deposit indicates a steady waxing then waning of eruption intensity. The generation of the K11 mLT following the waning of the eruption column, and the locally gradational contact between the two facies suggests that a PDC was generated by the collapse of the eruption column. The variably gradiational/sharp nature of this boundary indicates spatially variable sedimentation versus over-passing conditions within the density current [e.g. Branney and Kokelaar 2002; Brown et al. 2003; Doronzo et al. 2010]. The vertical and lateral grading of the mLT into a dxST implies deposition from a sustained but increasingly dilute PDC with time, and the lobate bedding structures with distance implies an increased flow unsteadiness distally. The eruption ended with the emplacement of a silicic lava, gen-

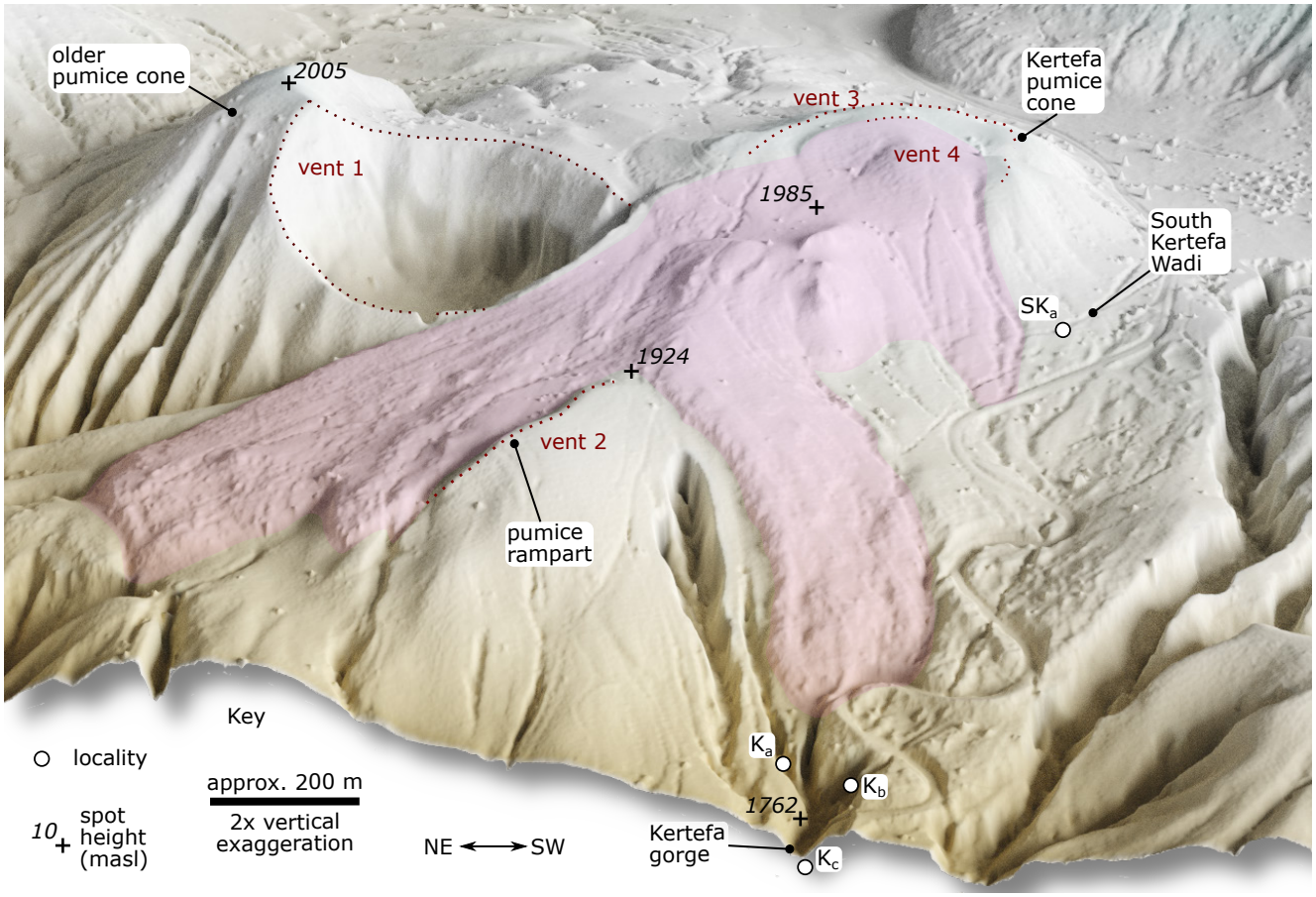

Figure 4: Overview of the Kertefa Pumice Cone Complex, showing the main features of the complex and the locations of field sites discussed here. Silicic lava (K12) is highlighted in pink. Topographic data is 2 m LiDAR from [Hutchison et al. 2014]. The KPCC is located on the NW flank of Aluto's edifice (see Figure 1). The 200 m scale bar is calibrated to the foreground.

erating a lower autobreccia, with a more ductile glassy and microvesicular core. The presence of pink pumices from the mLBr in the base of the lava implies that the intervening PDC did not deposit further upslope, and indicates that there was no palaeosol between the PDC deposits and the lava.

KPCC 3: The 'Qup' eruption The 'Qup' eruption, as described by Fontijn et al. [2018], comprises a decimeter-scale bL fall deposit, high in the stratigraphy in the NW region of Aluto. We are unable to definitively attribute the Qup eruption to a particular pumice cone. However, it is likely to be from the vicinity of the KPCC, consistent with the isopachs of the Qup fall deposit [Fontijn et al. 2018]. The Qup fall deposit (K14) is found at the top of the Kertefa Gorge section, and near the top of the South Kertefa Wadi section which cuts into the flank of a the main pumice rampart (Figure 5A SK_a,d). Below the Qup fall deposit is a xsLT (K13) and above is a dsLT (K15). These are the final proximally exposed primary products of the eruption. The sequence is incised by narrow (< 1 m), shallow (< 0.5 m) steep-sided rills and box-shaped gullies filled by cross stratified, granule-sized, pumice and lithic-bearing deposits (K16). This transforms upwards into a regolith and modern soil (K17). The xsLT and dsLT are interpreted as deposits of PDCs which possessed high and lower concentrations of particles within their respective lower flow boundary zones. The presence of two flow deposits, with an intervening decimeter-scale bedded, regional-scale fall deposit implies an unsteady eruption that generated an eruption column that repeatedly collapsed to generate PDCs. The K16 deposits are thought to be volcaniclastic, representing the remobilisation of pyroclastic sediment by water as hyperconcentrated flows and normal streamflows.

3.3.1 *Humo Gorge*

Humo gorge and the surrounding regions record at least three eruptions within the SW corner of the interior of Aluto caldera (Figure 1). The first and third are well exposed, with identifiable pumice cones. The second is less well constrained, and comprises gorge-filling pyroclastic deposits from an unknown source. The deposits are all stratigraphically below a lava flow dated to 61 ± 8 ka [Hutchison et al. 2016b]. An overview of the structure of Humo gorge, and the locations of the products of each eruption are shown in Figure 6.

Humo 1 eruption The stratigraphically lowest units exposed around Humo gorge are not separated by palaeosols, and so are considered to be produced by a single pumice cone eruption, which has developed a largely eroded and partially buried shallow pumice cone. Humo gorge cuts across the

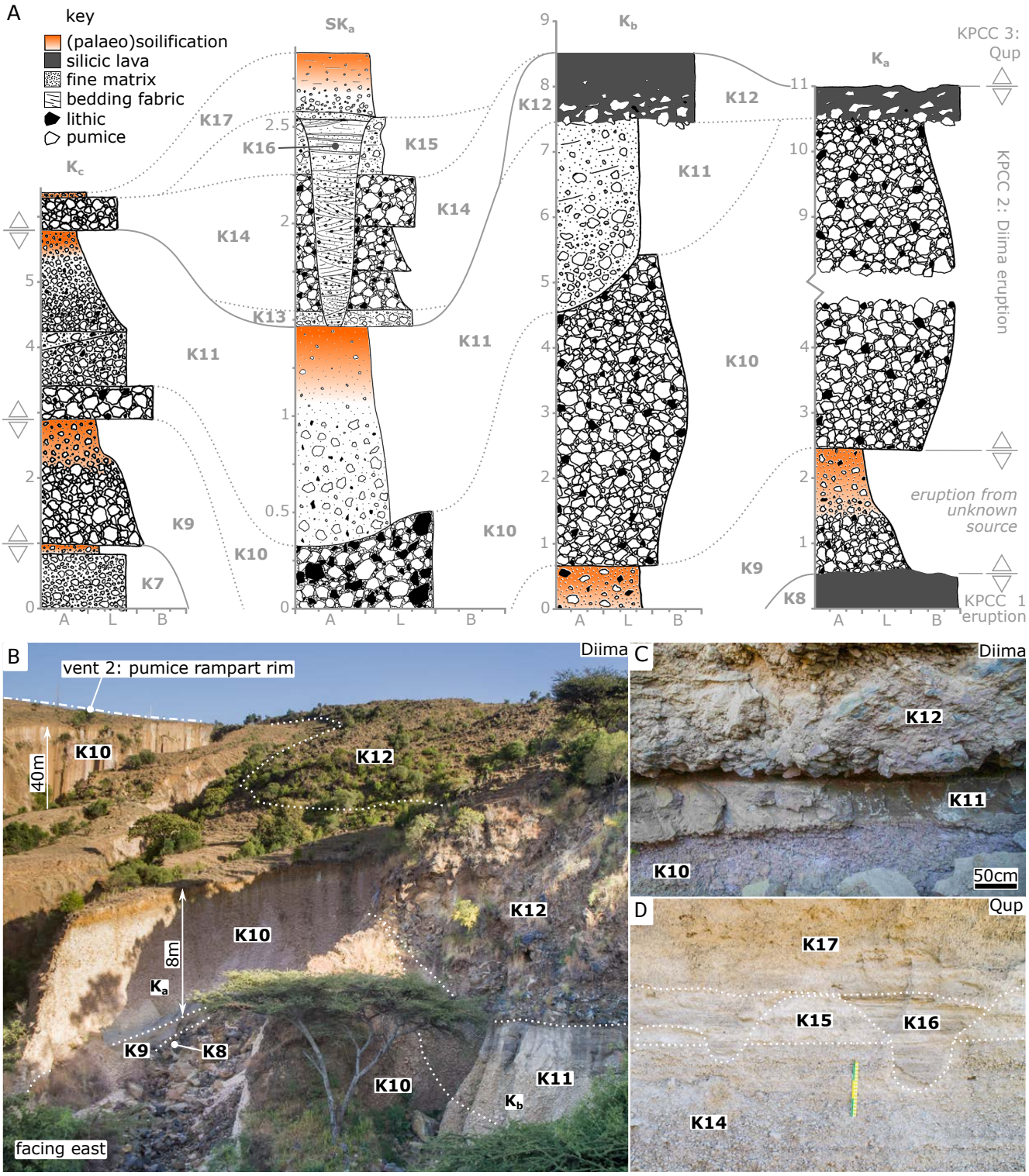

Figure 5: Pyroclastic logs and images of the KPCC deposits. [A] Pyroclastic logs and correlations of the KPCC from Kertefa gorge and South Kertefa Wadi. Key indicates symbology. Degree of rounding, clast support, bedding structure and grain size are communicated qualitatively by modification of these symbols. The symbology is reflective of all logs in this work. Log locations are in Figure 4. Logs from left to right represent distal to proximal pumice cone deposits. Note the expanded vertical scale of log SK$_a$. [B] Overview of Kertefa gorge showing the field relations of the Diima eruption deposits; from the base marked by an palaeosol (upper K9), to the emplacement of the Diima silicic lava (K12). [C] The deposit transitions from mLBr (K10), to xsLT (upper K11), to the emplacement of an autobrecciated silicic lava (K12) representing the waning phase of the Diima eruption. [D] Upper deposits from South Kertefa Wadi showing the transition from the bL 'Qup' fall deposit (K14), to dsLT ignimbrite (K15), rill-filling volcaniclastic deposits (K16), and finally a regolith and modern soil (K17). The scale is 30 cm long.

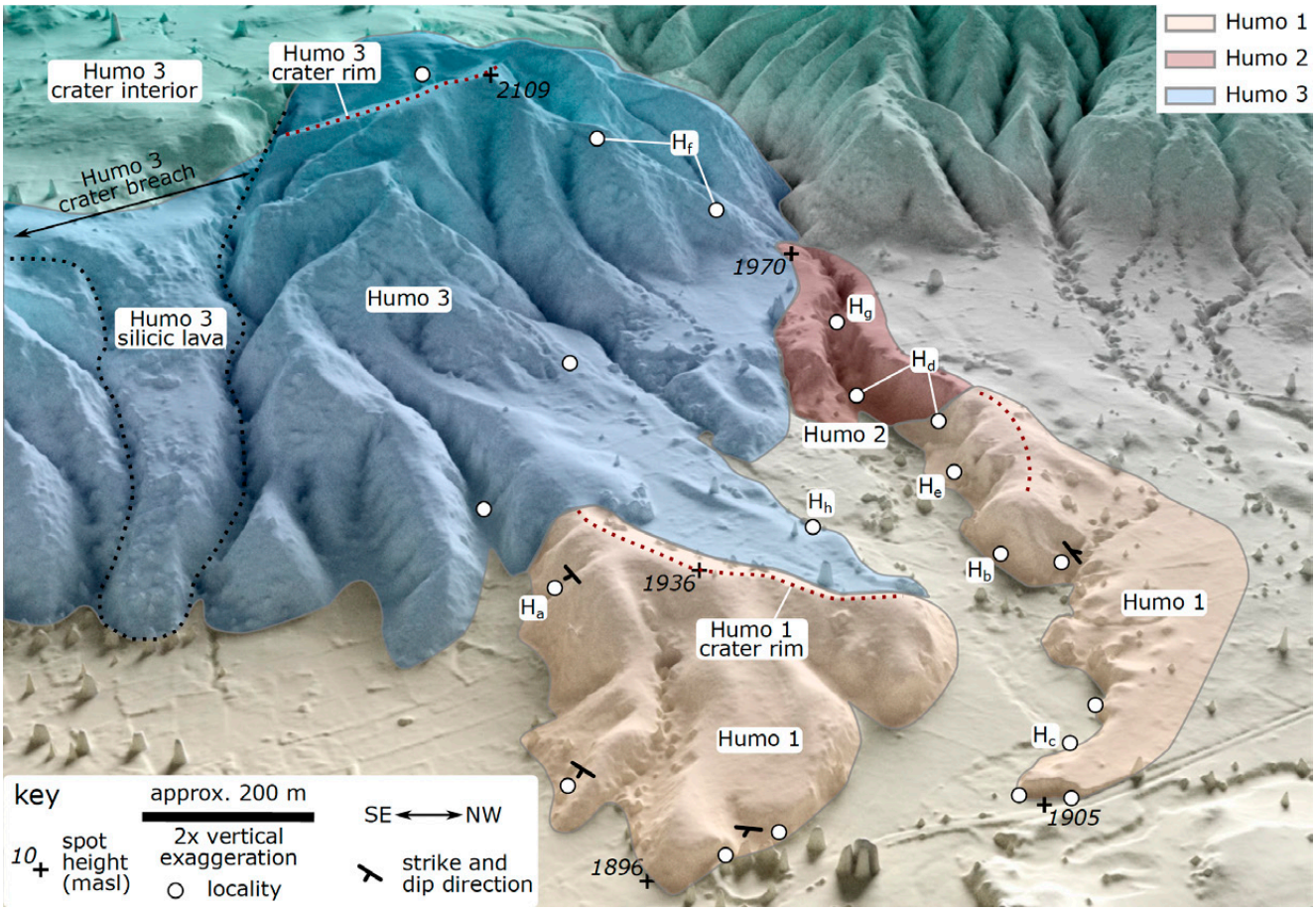

Figure 6: Overview of the Humo gorge region and field sites. The deposits and structures from the three main eruptions are shown. Humo 1 and 3 pumice cones, and their crater rims, are visible. The source of the KPPC 2 eruptive products is uncertain, but is likely to be somewhere further south and uphill from Humo gorge where the deposits are currently preserved. The scale bar is calibrated to the foreground.

pumice cone, providing a cross-section of the deposit stratigraphy (Figure 6). A subset of the pyroclastic logs is shown in Figure 7A. The remains of the cone are broad and short (apparent crater diameter ≈450 m, height ≈40 m), though highly eroded, making it challenging to assert an original morphology. The Humo 1 pumice cone is built from two mLBrs at the base (H2 and H5), and towards the top bLBr (H6) that dip between 28 and 32° away from the cone centre at and become qualitatively more lithic poor with height (Figure 7). Stratigraphically above this, and away from the cone slopes, more distal exposures comprise matrix-rich mLTs that onlap the cone slopes (H7 and H8). The sequence is topped by a modern soil. There is no exposed silicic lava from the Humo 1 eruption, though the cone has apparently undergone extensive erosion and burial which may erase or obscure such a feature. The cone itself is interpreted as the accumulation of tephra fall around the vent. The presence of two sharp bedding surfaces within the mLBr facies implies discontinuities in fall deposition, perhaps by pauses in the eruption. However, this separates only three multi-meter scale massive beds and so each phase is considered to be steady, rather than pulsatory. With time, the cone became sufficiently steep to develop the bLBr facies. This was followed by the generation of PDCs, which in stratigraphic context, and by their componentry, is most commensurate with column-collapse.

Humo 2 eruption The Humo 2 eruption is recorded as a series of gorge-filling pyroclastic deposits (H9 to H16, Figure 7B). The first deposit is a mLBr (H9) containing out-sized pumice blocks. This is followed by a dxsLT (H10), and a further mLBr (H11), better sorted than H9 without outsized blocks. This is followed by thick (≤ 20 m), gorge-filling ignimbrites and co-ignimbrite sTs (H12 to H16). H12 and H13 are mLTs, with an overlying fine co-ignimbrite sT (H14), followed by a dxsLT (H15) with a further co-ignimbrite sT (H16). The mLBrs are fall deposits, with the presence of outsized pumice blocks suggesting either that they are close to source, or considering they are filling gorges, may have fallen in from the gorge walls. These deposits are not themselves cone-forming (as they fill a gorge) but may or may not be associated with the cone-forming phase of a pumice cone eruption. The intervening mLT (H10), indicates the eruption column that generated the fall deposits was unsteady, generating a PDC. The following ignimbrites and co-ignimbrite ash falls indicate further PDC forming episodes with intervening quiescent periods allowing ash to settle. This is consistent with either an

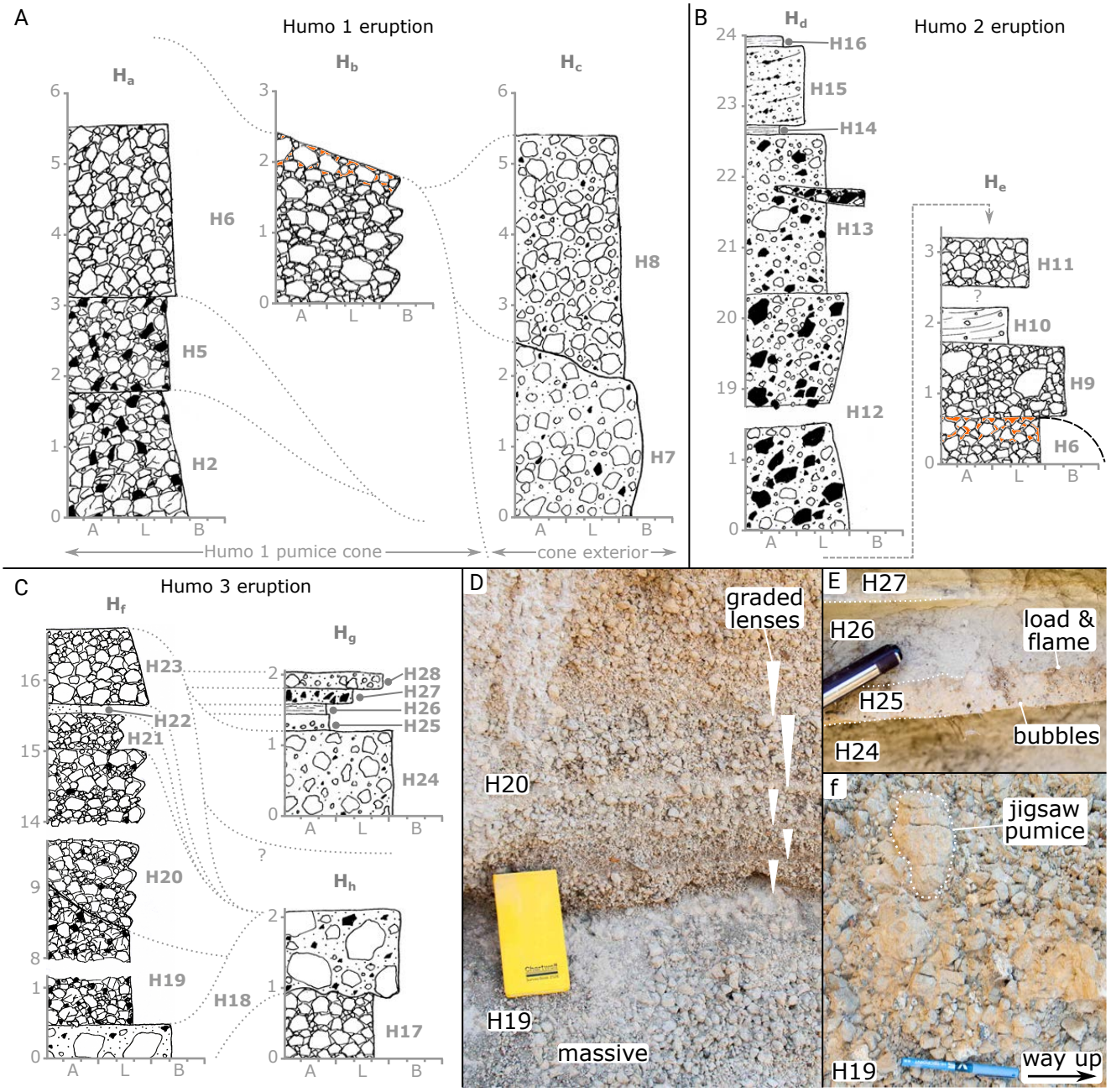

Figure 7: Logs and images of the Humo gorge deposits. [A] Logs of Humo 1 eruption deposits. The location of the logs are cross referenced in Figure 6. [B] Logs of Humo 2 eruption deposits. [C] Logs of Humo 3 eruption deposits. [D] The transition between lower massive pumice breccia forming a shallow cone, and inversely graded, lensoid beds of pumice breccia; representing granular flow-modified fall on the outer repose slope of the Humo 3 pumice cone. Taken at the location of log H_f. [E] Deposits at the end Humo 3 eruption, filling the Humo 1 crater. Showing clear indications of water laden density currents and sediments (bubbles in ash, load and flame structures), followed by the settling out of fines through still water (planar laminations). Taken at the location of log H_g. [F] Typical massive pumice breccia forming a short and wide pumice cone, including [fractured, but intact] 'jigsaw' pumices; indicating no post-depositional transport. There is a notable lack of such pumices in the lenticular bedded pumice breccias in the upper portions of the cone. Taken near the location of log H_f.

unsteady, pulsatory eruption, without the formation of stable eruption columns between PDC generation events (i.e. vulcanian blasts), or the generation of deposit-derived PDCs from unstable pyroclastic deposits after the main eruption event [e.g. Risica et al. 2022]. Due to a lack of exposure, further details of this eruption, including the location of the vent, are unknown.

Humo 3 eruption The Humo 3 eruption comprises a tall pumice cone (139 m minimum), outflow facies, and a (now buried) silicic lava flow (Figures 6 and 7C). Small remnants of crater-rim can be identified in the DSM, with an in-filled crater forming a plateau to the south, and an outer flank of the cone forming the main slope into the caldera. The cone

is now deeply incised by deep v-shaped gullies, and an extensive road-cut; providing excellent exposure of the bulk of the pumice cone. The main body of the cone comprises mLBr (H17, and H19) with a thin mLT (H18), which grades upwards into a series of steeply bedded bLBrs (H20 to H21). Towards the top of the cone, there is a massive fine ash (H22) and a normally graded mLBr (H23). Stratigraphically above these deposits, on the lower flanks of the cone (and filling the crater of the Humo 1 cone), is a mLT (H24) and a series of deposits (H25 to H28) (Figure 7E), including an mT with matrix bubbles (H25), an mT with a loaded base that grades upwards into a planar sT (H26), followed by two thin indurated breccias (H27 and H28). The final primary product of the eruption is a now-buried silicic lava, identifiable in the DSM, and with poor and sporadic exposure, but appears to have flowed through a breached flank of the cone. The main cone was built by the accumulation of tephra fall around the vent, forming a thick massive deposit, with the occasional intervening collapse event generating PDCs. As the eruption progressed, the cone-slopes steepened to the angle of repose. The presence of more extensive planar bedding surfaces in the succession implies the eruption was not entirely continuous, and towards the end was unsteady and waning, depositing finer-grained fall deposits. The later stages of the eruption were marked by the generation of another PDC, which by-passed the cone slopes depositing beyond the break in slope at the base of the cone, and finally by the emplacement of a silicic lava. The series of deposits filling the Humo 1 crater, stratigraphically above the lava flow, were evidently deposited with a high proportion of water accounting for soft sediment deformation structures and matrix bubbles. It is possible that H25 is a vesiculated tuff emplaced by a PDC generated by phreatomagmatic explosions, or alternatively that the package represents a series of volcaniclastic sediments emplaced by or through a body of water. In either case, these deposits indicate the Humo 3 eruption occurred in a humid environment, with potential for hydrovolcanic actvity.

3.3.2 *Awariftu valley*

Awariftu valley, on the northern outer flank of Aluto, provides lateral exposure of at least two eruptions separated by a palaeosol (Figure 8). The Awariftu 1 and Awariftu 2 deposits (Figure 9), forming the southern end and eastern side of the valley onlap the dated pumice cone on the western side of the valley, indicating that these are the youngest eruptions from Awariftu valley, and are $< 18 \pm 8$ ka [Hutchison et al. 2016b].

Awariftu 1 eruption The first eruption produced a short (≈45 m), wide (apparent crater diameter ≈400 m) pumice cone at the head of Awariftu valley (Figure 8). The cone comprises a mLBr (A1), with a a high proportion (20–40 vol.%) of deposit-quenched pumiceous achneliths (DQAs, Figure 9b), with an overlying matrix-poor mLT/mBT with a fine grained base, and becomes more matrix rich distally (A2). The mLT/mBT has an undulating upper surface, which is filled in proximal locations by a lithic-rich angular breccia with a muddy matrix (A4), and at distal locations by a low-angle cross-bedded, muddy, indurated deposit with laminations of lithics and pumices (A3) followed by A4. Above this is a mLT (A5) capped by a palaeosol. There is no known obsidian lava associated with this eruption. Typical of many cones at Aluto, the first deposits of the pumice cone are proximal mLBr fall deposits around the vent which form the main body of the cone. The lapilli-sized DQAs represent fluidal juvenile material falling from the turbulent edge of an ascending eruption column, without sufficient time to cool through their glass transition, but too small and low density to be deposited ballistically [Clarke et al. 2019]. The following mLT/mBT indicates this column then collapsed, generating a coarse-grained PDC with elutriated fines, and little opportunity to generate fines through comminution of pumice. This was followed by the generation of a lahar, first depositing A3 by a hyperconcentrated flow, then a coarser debris flow deposit (A4); a common sequence generated by progressive aggradation of lahar deposits [Pierson and Scott 1985; Vallance and Iverson 2015].

Awariftu 2 eruption The Awariftu 2 eruption began with the deposition of a tall pumice cone (> 200 m), which forms the eastern side of Awariftu valley (Figure 8). The bulk of the pumice cone comprises mLBr (A6), with <10 vol.% DQAs. This is followed by a complex stratigraphy of several matrix-poor and matrix-rich mLTs, dbLTs and xsTs which can be traced along a road cut through the slopes of the pumice cone, and into the valley itself. A particularly lithic-rich clast-supported mLT (A10) followed by a mT to dbT with sparse accretionary lapilli (Figure 9C, 9D) provides a marker sequence to permit correlation. Small discontinuous beds of clast-supported open-work angular pumice lapilli, with eroded upper surfaces (e.g. A19, A17) can be found within the sequence of matrix-bearing deposits. The sequence ends with a series of matrix-supported mLTs, the last with a coarse lithic-rich base containing DQAs. There is a crystal rich silicic lava flow from the main vent of the Awariftu 2 cone visible in the DSM that flows over the stratigraphy (Figure 8). Following the sequence of events at other Aluto pumice cones, the cone develops first as an accumulation of mLBr tephra fall around the vent. The Awariftu 2 cone did not reach sufficient steepness for repose-slope grainflow, so the bLBr facies has not been observed. The following series of matrix bearing deposits indicate the collapse of the pyroclastic eruption column to generate PDCs. The sections investigated here are very close to the vent (≈300 m) and on the outer cone slope, and the presence of particularly matrix-poor and lithic-rich PDC deposits might represent the impact zone of descending tephra. The presence of beds of sparsely preserved open-work angular pumice lapilli indicate occasional resumption of deposit accumulation by tephra fall. While open-work pumice-rich ignimbrite facies do exist (marking the levees of flow-lobes [Branney and Kokelaar 2002]), the pumice lapilli in the Awariftu 2 beds are distinctly angular compared to the surrounding flow deposits, indicating a lack of comminution, and so are interpreted as fall deposits. This repeated intercalation of tephra fall and PDC deposits indicates either a sustained eruption column with repeated partial collapses (generating PDCs that variably erode accumulated tephra fall), or repeated explosive phases that temporarily form a stable column, fol-

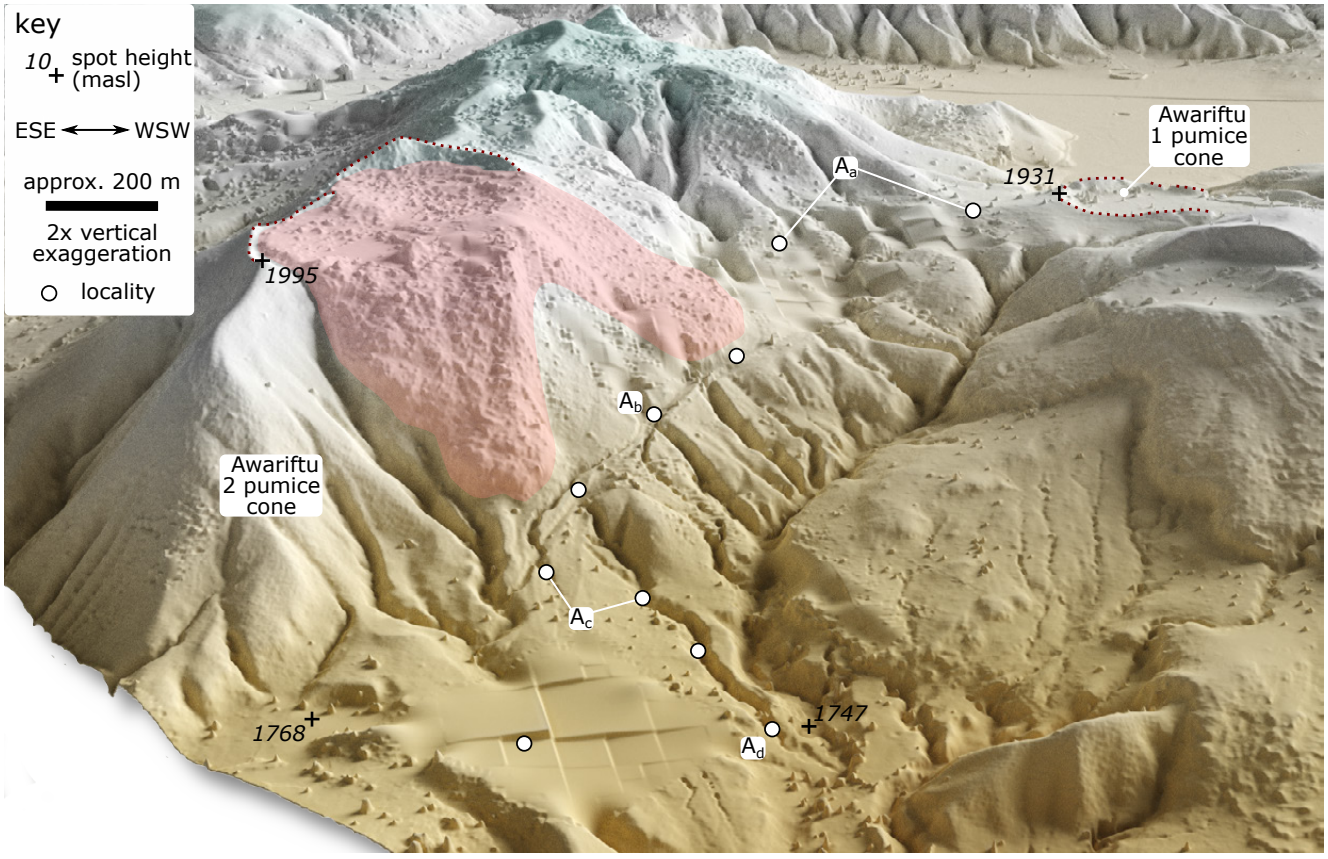

Figure 8: Overview of the Awariftu valley and field sites, facing SSW into the caldera. The deposits and structures from the two studied Awariftu eruptions are shown. Onlapping relations indicate that the cones and lavas visible on the western side of Awariftu valley (right of image) are older than the Awariftu 1 and 2 deposits. The Awariftu 2 lava is highlighted in pink. The scale is calibrated to the foreground. Regular squares in the topography are artefacts from repairs to the LiDAR data set.

lowed by wholesale column collapse. The sparse accretionary lapilli (as opposed to pellets) in the mT/dbT indicate a flow origin, the presence of moisture to nucleate pellet formation in a co-ignimbrite plume, and the growth of accretionary lapilli in a fine grained density current [Brown et al. 2010]. This and the syn-eruptive presence of lahars, indicates a humid environment. While it is possible the fine grained accretionary lapilli-bearing deposit might represent a hydrovolcanic phase, there is little evidence for any prolonged magma-water interaction in the rest of the Awariftu 2 deposits. The eruption ended with the emplacement of a silicic lava.

3.3.3 *Central, Quarry and Gabiben Pumice Cones*

The Quarry and Central pumice cones are connected eruptive centres along the Artu Jawe fault zone within Aluto's caldera (Figure 10). Superposition indicates that the Central pumice cone erupted first, followed by the Quarry cone, though the length of time between these eruptions is uncertain. The Gabiben pumice cone in the NW of the caldera floor is the youngest primary volcanic feature in the local area, but there are no absolute age constraints.

Central pumice cone The deposits of the Central pumice cone are relatively poorly exposed, but comprise a mLBr with abundant DQAs, forming an asymmetrical ring approximately 30 m tall with an apparent crater diameter of 500 m. These are the only pyroclastic deposits from the central cone exposed; and any further deposits are likely to form flat farmland to the West. The end of the Central Cone eruption is marked by a comparatively small silicic lava sitting in a small breached saddle on the southern rim of the pumice cone, with visible surface ogives that converge on the centre of the saddle (Figure 10, Central Cone lava). The eastern rim of the Central pumice cone crater is incised by a box-shaped gorge filled with a silicic lava (Figure 9, Quarry Cone lava) that emanates from a vent associated with the Quarry pumice cone. The Quarry Cone lava stops abruptly, forming a shear face concordant with the interior slope of the central pumice cone. The floor of the cone is partially covered by a debris fan (observable in the elevation model and sparsely exposed) which thickens towards the gorge at the inner eastern wall of the cone toward the breach. A steeper, inactive talus slope comprising obsidian blocks sits at the base of the Quarry Cone lava, partially burying the debris fan. The structure of this cone is unusual, but highlights important processes that evidently occur at Aluto pumice cones. Firstly, the asymmetry of the cone might indicate a relatively weak eruption plume (bent over by wind to the NE) [e.g. Dawson and Powell 1969; Valentine et al. 2007; Mattsson and Tripoli 2011], or a directed eruption from an inclined conduit [e.g. Zanon et al. 2009; Graettinger et al. 2015].

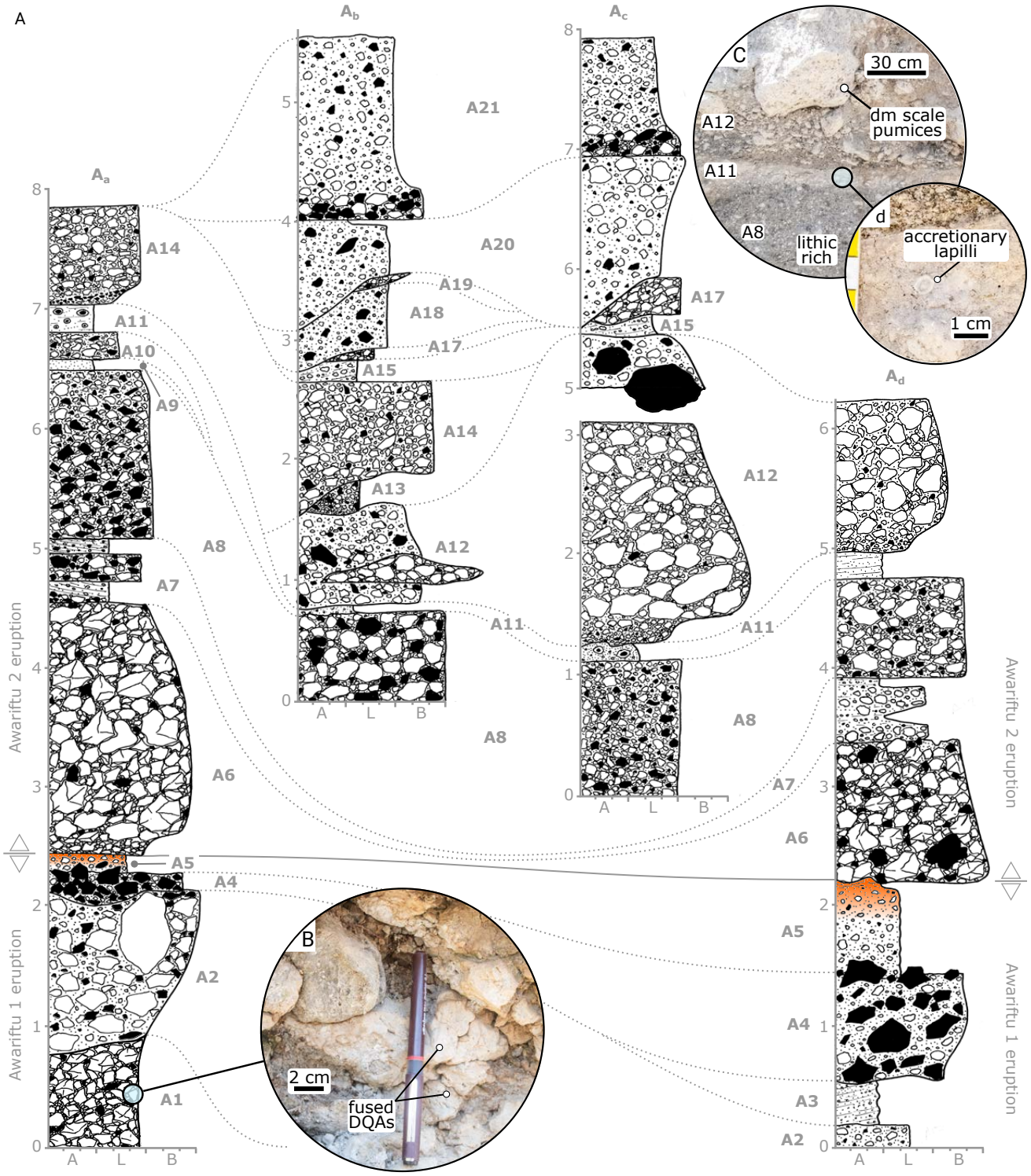

Figure 9: Correlated logs and images of the Awariftu 1 and 2 pumice cone eruption deposits. [A] Logs of the Awariftu 1 (A1 to A5) and Awariftu 2 (A6 to A21) deposits exposed along Awartiftu valley. An obsidian lava from the Awariftu 2 eruption can be found on the western flank of the Awariftu 2 pumice cone, set back from the exposures described here (Figure 8). Height scale is in meters above the base of the exposure. [B] Image of the A1, Awariftu 1, pumice cone building fall deposit containing numerous fused DQAs (deposit quenched achneliths). These pyroclasts display in-situ inflation within the deposit. Their plastic behaviour indicates their short flight-time to the deposit, ultimately indicating their source from the edge of an ascending eruption column [Clarke et al. 2019]. [C] Overview of the stratigraphic marker units: lithic-rich A8, ash rich and accretionary lapilli bearing A11, and large pumice-rich ignimbrite A12. [D] Inset of an accretionary lapillus within unit A11.

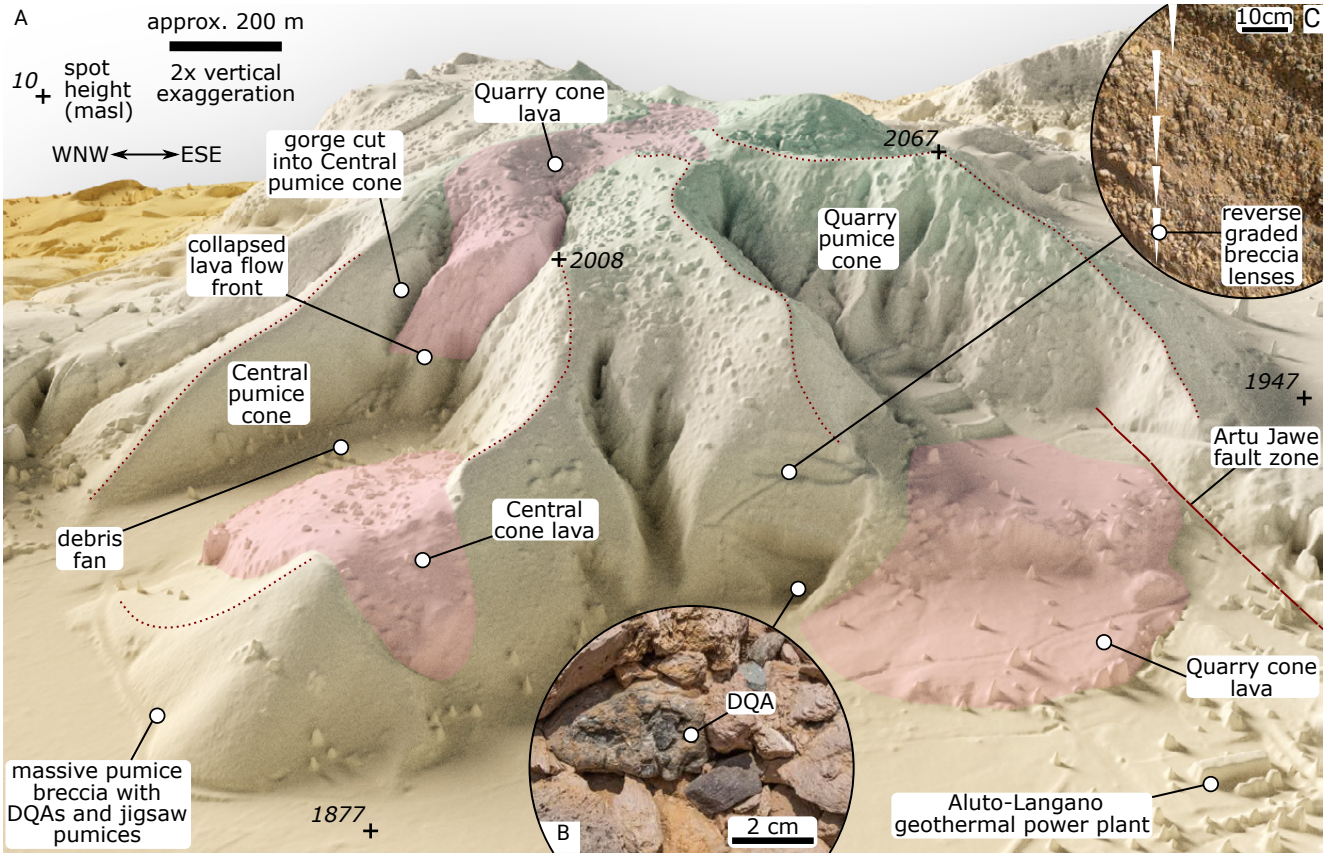

Figure 10: An overview of the Central and Quarry pumice cones. [A] Showing the key relationships between, and features of the Central pumice cone and silicic lava, followed by the Quarry pumice cone and lava. The scale is calibrated to the foreground. [B] Photograph showing the massive pumice breccia forming the lower stratigraphy of the Quarry pumice cone, including a DQA pyroclast [Clarke et al. 2019]. [C] Photograph showing the steeply bedded, inversely graded lensoid beds of pumice breccia that form the upper stratigraphy of the Quarry pumice cone.

Secondly, the emplacement of lava from the crater rim, and not from the central eruption vent is unusual. The presence of surface ogives indicates that the present day lava surface is original, and not an erosional remnant of a flow sourced from elsewhere. The high point of the lava and converging ogives indicate the location of the vent, which is SW of the main central cone vent. This is consistent with the strike of faults and pumice ramparts at Aluto, suggesting the eruption was dyke-fed, with a small secondary vent developing along strike close to the main vent. Moreover, the location of this lava challenges, at least in this case, formation by the extrusion of accumulated sintered pyroclastic material against the wall of a vent, as there is no pyroclastic cone centred on the saddle. If the obsidian lava is the product of viscous sintering, this must have taken place immediately upon vent opening, with little or no surface explosive activity. Finally, the arrested Quarry Cone lava indicates that similar to basaltic scoria cones [Sumner 1998; Németh et al. 2011], pumice cones are unstable and can undergo lava-induced collapse. The inferred process of collapse is shown in Figure 11; where the inflation or growth of the Quarry Cone silicic lava against the outer wall of the Central pumice cone continued until the wall failed, allowing the silicic lava to partially advance and the lava flow front to collapse forming a talus slope.

Quarry pumice cone The Quarry pumice cone is an elongate pumice rampart that is situated directly above, and follows the strike of the Artu Jawe fault zone; on an en-echelon lineament to the Awartftu 2 cone. The rampart rises to a height of ~100 m above the caldera floor. A series of quarries in the outer western flank of the rampart expose a clear stratigraphy of mLBr to bLBr facies (Figure 10). The base of the quarry, marking the earliest deposits of the eruption, comprises a mLBr with abundant DQAs (Figure 10B). This grades with stratigraphic height into a bLBr facies without DQAs, best exposed in the upper quarry (Figure 10C). These are the only known pyroclastic deposits of this cone, as there is no traceable distal exposure. A shallow-buried silicic lava is apparent in the DSM (Figure 10). The lava is tentatively associated with the Quarry Cone lava at the top of the pumice cone, though the intervening exposure has been removed by earthworks associated with the Aluto-Langano geothermal power station. The temporal and eruptive relationship between the Quarry Cone and Awariftu cone is unknown, and it is possible that they developed during the same eruption. The burial of the Quarry Cone lava suggests it post-dates the exposed Awariftu 2 lava.

Gabiben pumice cone The Gabiben pumice cone (Figure 12) is a shallow (≈50 m tall), wide (apparent crater diameter ≈550 m), asymmetric pumice cone, which lies along a NE/SW striking fault [Hutchison et al. 2015], from which emanate a series of three crystal-rich obsidian lava flows along a distance of 2.75 km. The pumice cone itself comprises mLBr, though overall, exposure is poor. There are two subsidiary craters, also along a NE/SW strike, which appear excavated, rather than constructed. Eruption began at the SW end of the lineament forming the main cone by tephra fall around the vent, which was then partially excavated by phreatic explosions to the NE forming the two subsidiary craters. The relative timings of the three silicic lavas is unknown, but considering the SW to NE progression at the main cone, this may be mirrored in the temporal sequence of lavas along strike. The linear series of vents, like many at Aluto, suggest the pumice cone eruptions are dyke-fed.

4 Discussion

4.1 A comparison with the distal tephra record

Terrestrial and lacustrine sediments exposed in gorges ca. 5–10 km to the West of Aluto, as well as lake sediment cores from Lakes Abijata and Langano (25 and 15 km to the South of Aluto respectively) provide a record of distal tephras from Aluto eruptions throughout the Late Pleistocene and Holocene

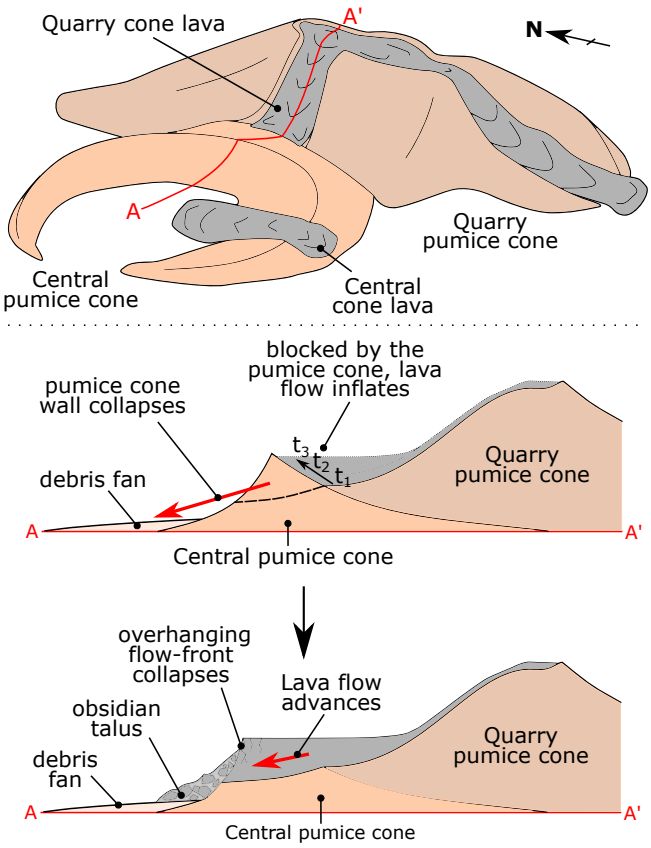

Figure 11: Schematic diagram showing the process leading to the partial collapse of Central pumice cone by the emplacement of the Quarry cone silicic lava.

[Fontijn et al. 2018; McNamara et al. 2018]. In the gorges, the predominant facies is clast-supported mL pumice, typically up to a few cm to a few dm in thickness, and which have been interpreted as medial-distal fall deposits of explosive eruptions at Aluto, as also confirmed by their glass chemical composition [Fontijn et al. 2018; McNamara et al. 2018]. Sometimes the fall deposits transform upwards into a more fines-enriched mLT facies, occasionally displaying low-angle cross-bedding, and this has been interpreted to either reflect distal PDCs, or (syn-eruptive) remobilisation into a (palaeo)lake [Fontijn et al. 2018]. Consistent with our observation of cone-building rather than sheet-forming fall deposits, is that the few fall deposits that have been laterally correlated thin out relatively quickly, with tentative half-distance thickness (b_t) values Pyle [1989] of <1 km [Fontijn et al. 2018]. Lake sediment cores contain numerous (24 in Lake Abijata; 19 in Lake Langano) ash layers geochemically correlated to Aluto. They are typically on the order of 1–3 cm thick and fine grained (M_d on the order of 2–3 ϕ), with the exception of one 11 cm thick and coarser tephra in Lake Abijata. These are interpreted as primary fallout from moderate-magnitude (M ≈ 4) explosive eruptions at Aluto [McNamara et al. 2018]. Important to note, is that Lake Tilo sediments (ca. 110 km SSW of Aluto) contain two fine ash layers (0.5–1 cm thick) that have a chemical composition consistent with that of other Aluto tephras. McNamara et al. [2018] tentatively suggested that one of these units could correspond to the thickest tephra in Lake Abijata, and possibly represent an eruption of Plinian magnitude from Aluto. Considering the near absence of absolute age constraints for proximal deposits, the geochemical homogeneity of juvenile compositions, and the selective recording of only moderate-to-high-intensity explosive eruption deposits in lake cores, it remains very challenging to integrate the terrestrial and lacustrine records at Aluto. Nonetheless, the record is consistent with observations of the proximal deposits, that pumice cone eruptions comprise a sustained but unstable eruption column leading to (with important exceptions) rapidly thinning, moderately widespread tephra deposition.

4.1.1 *PDC generation mechanisms at Aluto pumice cones*

PDC deposits from Aluto pumice cones lack the high proportion of dense, low-vesicularity blocks of lava typical of block and ash flows derived from dome and flow-front collapse [e.g. Cole et al. 2002]. Their heterogeneous lithic population (including many sub-volcanic sedimentary clasts, sourced from deep in the conduit and below), and abundance of pumice, is also inconsistent with PDCs derived from such generation mechanisms [e.g. Cole et al. 2002]. This perhaps reflects the tendency of peralkaline rhyolites to form more-stable shallow domes and flows [e.g. Hunt et al. 2019], rather than steep domes or spines. However, piling of silicic lavas against unstable barriers, as seen at Central pumice cone, could conceivably provide a mechanism for block-and-ash flow generation at Aluto. More generally, the PDC deposits at Aluto are most consistent with generation by column-collapse events, either as numerous distinct vulcanian blasts [e.g. Cole et al. 2014], or repeated partial collapses of a sustained eruption column [e.g. Taddeucci et al. 2004; Carazzo et al. 2020]. Vulcanian erup-

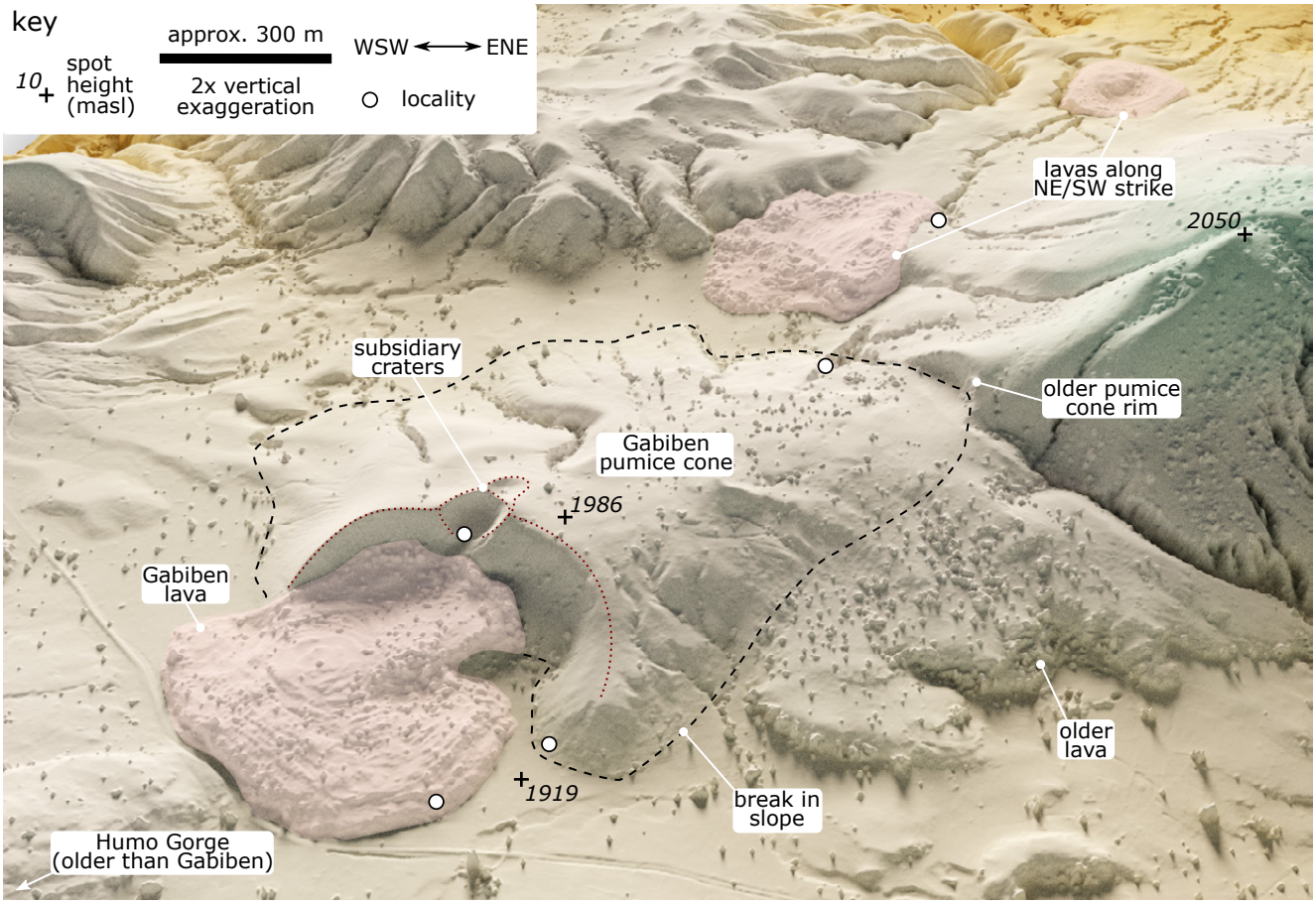

Figure 12: Overview of asymmetrical Gabiben pumice cone and the surrounding area. Showing the Gabiben pumice cone, delineated by a break in slope, the Gabiben lava, and associated lavas along strike (pink). By superposition, and lack of gullying, Gabiben appears to be the youngest eruption in the area.

tive products often contain dense juveniles such as breadcrust bombs, derived from dense conduit-blocking plugs [Woods 1995; Clarke et al. 2015]. Breadcrust bombs are present in some mLBr fall deposits at Aluto but are near-absent in the ignimbrites. However, glassy obsidian clasts are common, and could conceivably represent plug material. Then again, considering the abundance of obsidian lavas in Aluto's stratigraphy, they could alternatively be lithics derived from the conduit walls. Ignimbrite flow units at Aluto display strong stratigraphic variation in their granulometry, componentry, and inferred flow dynamics. Overall, this implies highly unsteady, pulsatory PDC generation mechanisms, rather than sustained column-collapse or boiling-over. The general lack of welding also implies somewhat greater pre-depositional cooling than would be expected from boil-over derived PDCs [e.g. Branney and Kokelaar 1992], especially considering the particularly low glass transition temperatures of peralkaline rhyolites [Dingwell et al. 1998; Di Genova et al. 2013], which should enhance welding processes at comparatively lower temperatures. This is in contrast to the commonly welded nature of peralkaline ignimbrites from larger-scale peralkaline rhyolite eruptions [Mahood 1984; Mahood et al. 1985; Mahood and Hildreth 1986; Williams et al. 2014]. The underlying mLBrs and bLBrs, themselves derived from sustained (though often unsteady) eruption columns, as well as the sometimes-gradational contact between these fall deposits and the overlying PDC deposits, suggests that repeated partial collapse of sustained but unsteady eruption columns are likely to be the typical source of PDCs at Aluto.

4.2 Pumice cone eruption sequences at Aluto

Though there are important differences between the pumice cone eruptions at Aluto, such as the degree of unsteadiness, and the size and morphology of the pumice cone produced, there are broad similarities between the sequence of events that occurred during each eruption. This is summarised in Figure 13, which compares the sequences of events for each eruption investigated here, and develops a conceptual model of a 'generalised' pumice cone eruption at Aluto. Though such a generalised eruption model inevitably simplifies the process of eruptions, it provides a useful conceptual framework on which to develop hazard assessments [e.g. Clarke et al. 2020; Tierz et al. 2020], and highlights the key events and processes that characterise pumice cone eruptions.

All pumice cone eruptions studied at Aluto begin with the deposition of a short pumice cone with a wide crater, and to a variable degree, more-widespread fall deposits, around the vent from a mixed-mode (ballistic, column-edge, umbrella

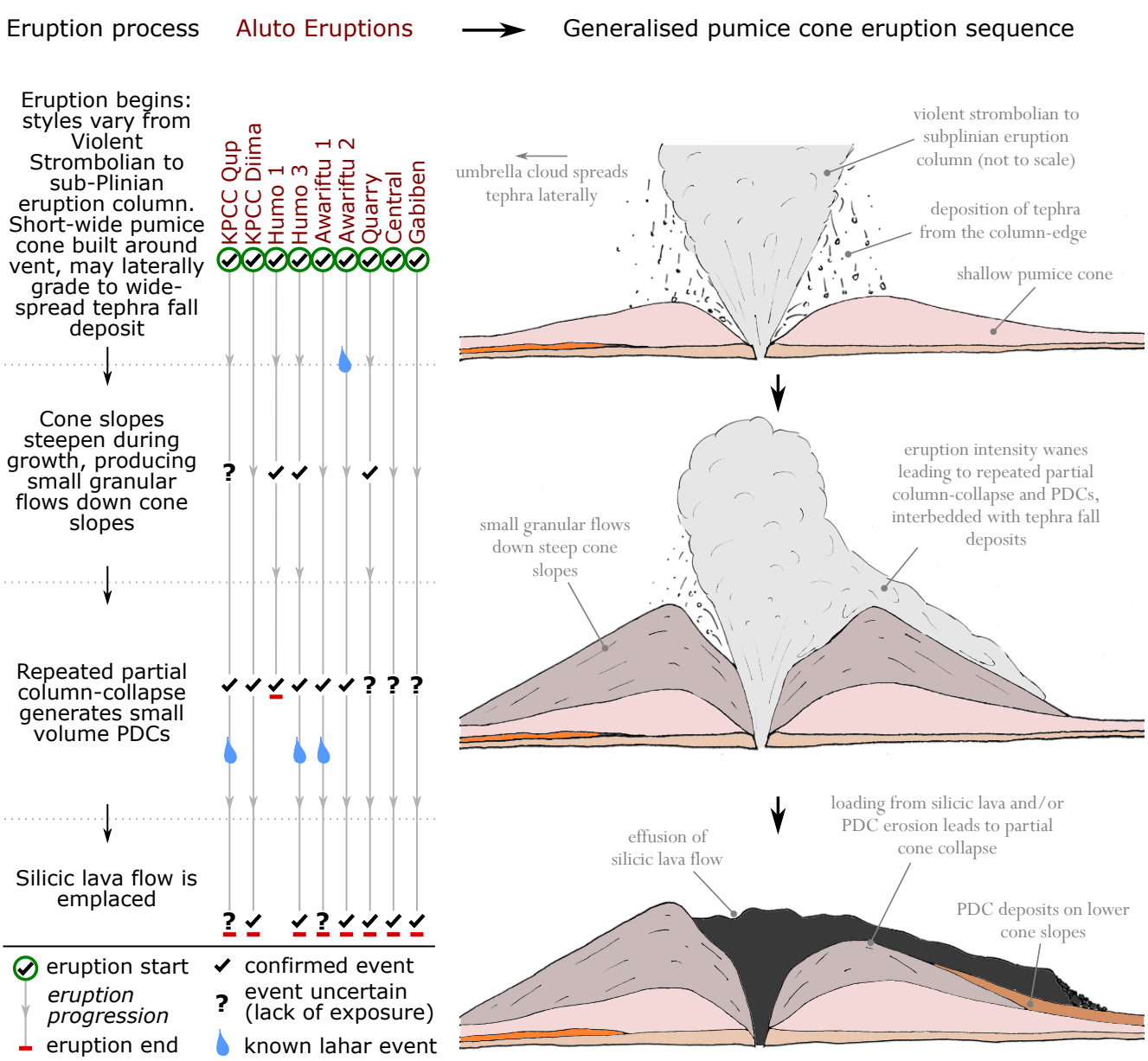

Figure 13: A generalised pumice cone eruption sequence [after, Clarke 2020; Clarke et al. 2020; Tierz et al. 2020] generated from the eruption sequences of Aluto pumice cones investigated here. KPCC 1, and Humo 2 are omitted as only the medial (non-cone forming) deposits have been found.

cloud) depositional regime. Occasionally, if this phase persists long enough for the cone slopes to steepen, small grain flows develop down the cone slopes in a similar fashion to the later stages of basaltic scoria cone eruptions [e.g. McGetchin et al. 1974; Sohn and Chough 1993]. The presence of elongate pumice ramparts, as well as aligned series of vents and lavas at Aluto implies many of the pumice cone eruptions are dyke-fed, and that a single eruption may produce multiple cones or lavas along strike. Given a sufficiently sustained eruption, these cones may merge to form ramparts. As the eruption intensity wanes, the eruption column becomes increasingly unstable, and likely partial-collapses of the eruption column generate PDCs. These PDCs tend to be concentrated currents with a fluid-escape or granular fluid–dominated lower flow boundary zones, and are often topographically constrained once they enter drainages. However, more dilute PDCs do occur, which may be less topographically confined. PDCs from pumice cone eruptions present a significant hazard to proximal and medial regions around Aluto [Clarke et al. 2020]. The final stage of the eruption is typically marked by the effusive emplacement of a silicic lava flow, which may or may not be accompanied by explosive activity.

Although lahars frequently occur during pumice cone eruptions at Aluto [this work, Clarke 2020], they are not included in the conceptual model, as their formation here is a function of rainfall, and therefore not intrinsic to the eruption process. However, they should be considered possible throughout and after these eruptions, particularly during Ethiopia's rainy seasons (*Belg* and *Kiremt*), where frequent intense rainfall often exceeds 40–50 mm h^{-1} near Aluto [Fazzini et al. 2015].

Table 2: A comparison of pumice cone-bearing volcanoes in the volcanic literature, where pumice cones are mentioned by name. This list is unlikely to be exhaustive, but pumice cones appear to be most often associated with volcanoes in extensional tectonic settings, that have undergone caldera collapse, and erupt highly evolved and/or highly alkaline magmas.

Volcano	Tectonic setting	Composition	Caldera present?	Key references
Aluto (Ethiopia)	continental rift	peralkaline rhyolite	yes	[Hutchison et al. 2015; Fontijn et al. 2018; Clarke et al. 2019; Clarke 2020]
Bora-Bericha (Ethiopia)	continental rift	peralkaline rhyolite	yes	[Fontijn et al. 2018; Tadesse et al. 2022]
Corbetti (Ethiopia)	continental rift	peralkaline rhyolite	yes	[Rapprich et al. 2016; Fontijn et al. 2018; Colby et al. 2022]
Furnas & Fogo (Azores, Portugal)	intra-plate	peralkaline trachyte	yes	[Cole et al. 1995; Wallenstein et al. 2015]
Gris cone—Cordon Caulle (Chile)	continental arc	rhyodacite-rhyolite	yes	[Lara et al. 2004]
Montaña Blanca (Tenerife, Spain)	intra-plate	phonolite	yes	[Ablay et al. 1995]
Monte-Pilato (Lipari, Italy)	graben	high-K rhyolite	no	[Dellino and Volpe 1995; Davì et al. 2011; Forni et al. 2013]
Newberry caldera (Oregon, USA)	back-arc basin	high-K rhyolite	yes	[Higgins 1969; 1973]
Pantelleria (Strait of Sicily, Italy)	submerged continental rift	peralkaline rhyolite	yes	[Mahood and Hildreth 1986; Orsi et al. 1989; Neave et al. 2012; Hughes et al. 2017]
Payún Matrú caldera (Argentina)	back-arc basin	trachyte	yes	[Hernando et al. 2019]
Pu'u Wa'awa'a (Hawaii, USA)	intra-plate	trachyte	yes	[Shea et al. 2017]
Sorocco island (Mexico)	abandoned mid-ocean-ridge	peralkaline rhyolite	yes	[Bryan 1966; Bohrson and Reid 1997]
Tuhua/Mayor Island (New Zealand)	extensional island-arc basin	peralkaline rhyolite	yes	[Ewart et al. 1968; Cole 1978; Houghton and Wilson 1989]

Lahar events observed in Aluto's stratigraphy are marked in the event sequence for each eruption in Figure 13. Similarly, though not intrinsic to the eruption process, the collapse of pumice cone structures, and thus the generation of avalanches (limited in volume to the size of the cone), and potentially block-and-ash flows, should also be considered possible during pumice cone eruptions, especially during lava flow effusion.

4.3 Aluto pumice cones in their global context

Pumice cones are not unique to Aluto, they have been described at volcanoes worldwide where they are commonly associated with extensional tectonic settings, highly evolved and/or alkali rich magma compositions, and with volcanoes that have previously undergone caldera collapse (Table 2). However, as a volcanic feature they remain imprecisely defined; and the term pumice cone is often applied in a broad, literal and subjective sense as an accumulation of pumiceous material in a cone or rampart around a vent. Consequently, pumice cones have been variously linked to a wide range of eruptive processes, from magmatic [this work, Orsi et al. 1989; Hughes et al. 2017; Clarke et al. 2019; Hernando et al. 2019, etc.] to hydrovolcanic [Cole et al. 1995; Dellino and Volpe 1995; Davì et al. 2011; Forni et al. 2013; Wallenstein et al. 2015], and from low intensity [Houghton and Wilson 1989; Orsi et al. 1989] to moderate intensity [Shea et al. 2017; Fontijn et al. 2018; McNamara et al. 2018; Clarke et al. 2019; Hernando et al. 2019], to high intensity [Higgins 1969; 1973] eruptions. Moreover, many proximal cones around vents associated with silicic eruptions could arguably be described as pumice cones, and share many features with the pumice cones investigated at Aluto and elsewhere. For example: the shallow cone surrounding the Quizapú 1932 Plinian vent of Cerro Azul, Chile [Hildreth and Drake 1992], the proximal cone surrounding the Novarupta 1912 vent, Alaska, USA [Houghton et al. 2004], and the shallow asymmetrical 'tephra cone' surrounding the Córdon Caulle 2011 Plinian eruption vent, Chile [Schipper et al. 2019], are similar in terms of their morphology, structure, granulometry and componentry to pumice cones investigated at Aluto, and reported elsewhere.

The process of building pumice cones was first attributed to ballistic accumulation of tephra around eruption vents, owing to their similarity in morphology and granulometry to basaltic scoria cones [Houghton and Wilson 1989]. However, the interpretation of basaltic scoria cones as purely ballistic Strombolian events is now considered inaccurate [e.g. Riedel et al. 2003; Valentine et al. 2005; Martin and Németh 2006; Pioli et al. 2008]. More recently, pumice cones have been associated with eruptions that have developed eruption columns, and workers have suggested that they represent the proximal accumulation of material falling from the edge of an eruption plume, in addition to a vent-derived ballistic component [Higgins 1969; Ablay et al. 1995; Clarke et al. 2019; Hernando et al. 2019]. This eruption column may be weak (low intensity) as shown by the low-dispersal Serra della Fastuca tephra (Pantelleria) [Orsi et al. 1989]. In other cases, the column may be strong, as shown by Newberry's central pumice cone [Higgins 1969; 1973], where the pumice cone is symmetrical, compared

to the highly asymmetric, wind-dispersed regional Plinian fall deposit of the same eruption. Globally, peralkaline rhyolite pumice cones are often associated with welded tephra fall facies, and display rapid vertical and lateral changes in welding intensity, from entirely unwelded and loose, to glassy and lava-like [e.g. Mahood and Hildreth 1986; Orsi et al. 1989; Houghton et al. 1992; Stevenson and Wilson 1997; Gottsmann and Dingwell 2002; Rotolo et al. 2017; Hernando et al. 2019]. Such features are characteristic of 'strongly peralkaline' magmas, where molar [NaO_2 + K_2O / Al_2O_3] (peralkalinity index) exceeds 1.1 [Mahood 1984]. Welding in peralkaline fall deposits has been attributed to a combination of low glass transition temperatures and little chance of pre-depositional cooling due to short collapse-heights (Hawaiian-like emplacement), and rapid accumulation rates [Mahood 1984; Gottsmann and Dingwell 2002]. Post-caldera pumice cone fall deposits at Aluto are conspicuously non-welded, despite a peralkalinity index of juveniles from several eruptions of 1.6 ± 0.12 (2 σ) [Hutchison et al. 2016b; Clarke et al. 2019], and high H_2O and F concentrations [Clarke et al. 2019; Iddon and Edmonds 2020], which act to lower melt viscosities and glass transition temperatures [Di Genova et al. 2013]. The ubiquitous lack of welding in Aluto pumice cone fall deposits, despite their geochemical and likely rheological similarity to other strongly peralkaline systems, implies somewhat more intense eruptions, generating taller columns associated with lower fall deposit accumulation rates, a greater opportunity for pre-depositional cooling [Sparks and Wright 1979], and without Hawaiian-like fountaining phases. The cause of this disparity remains uncertain.

The conditions required for the accumulation of a pumice cone, namely the proximal column-edge and ballistic deposition of pumiceous material, are not unusual, and so pumice cones can be generated by a diverse range of eruption styles and magnitudes globally, or at the same volcano. This has important implications for volcanic hazard assessment at volcanoes where pumice cones are found; though they indicate the existence of explosive, convective eruption plumes, careful interpretation needs to be made based on both proximal deposits and regional fall deposits to establish the particular intensity, magnitude and style of events any given pumice cone represents.

5 Summary

We have investigated the proximal deposits of at least nine pumice-cone-forming eruptions at Aluto volcano, Ethiopia. We have found that eruptions of these pumice cones are moderately intense explosive events that follow a similar eruptive sequence across a range of magnitudes. Importantly, pumice cone eruptions at Aluto are characterised by unsteady convective eruption columns that generate short and wide pumice cones that steepen as they grow. As the eruption intensity wanes, the eruption column undergoes repeated partial column-collapse, intermittently generating concentrated PDCs. The eruptions end with the emplacement of a silicic lava, but there may be continued hazard from lahars and small avalanches of pumice cone material well after the eruption. More generally, we suggest that many of the tephra fall deposits around the Main Ethiopian Rift may be the distal continuation of pumice cones, but that not all pumice cones generate wide-spread tephra fall deposits. Pumice cones themselves are interpreted as the product of mixed-mode deposition; from ballistic tephra, column-edge and umbrella-cloud deposition, that in some cases gives way to purely umbrella-cloud deposition at greater distances, similar to 'ultraproximal cones' described at Plinian eruption vents [Riedel et al. 2003]. The eruption case studies, and the generalised eruption sequence presented here provide important information to (1) characterise the eruption style of these enigmatic volcanic features, and (2) develop a conceptual model to inform qualitative and/or quantitative hazard assessments. [e.g. Clarke et al. 2020; Tierz et al. 2020].

Author Contributions

B.C authored the manuscript, with contributions from K.F; based on discussions with all authors. Field work was conducted by B.C, K.F, P.T, F.D., and E.S.C. Laboratory granulometry was conducted by B.C. G.Y provided practical and logistical assistance, and was instrumental in developing the RiftVolc project to which this work contributes.

Acknowledgements

We thank our field and logistical assistants Amdemichael Tadesse and Ermias Filfilu Gebru, as well as Vikki Smith, Sam Engwell, Keri McNamara and David Pyle for their assistance and discussions in the field. Thanks to our drivers: Solomon Getachew and Zelalem Mandefro, without whom our field work would have been impossible, and far less enjoyable. We thank the people of Aluto and surrounding regions, for your hospitality, access to your land, guidance, and assistance with field-sieving. We also thank Faysel Abdu for their translation of the abstract into Amharic. Published with permission of the Executive Director of British Geological Survey (NERC-UKRI). This work is a contribution to the Natural Environment Research Council (NERC) funded RiftVolc project (NE/L013932/1, Rift volcanism: past, present and future) through which E.S.C, K.F, P.T and G.Y were supported. In addition, B.C was funded by an Edinburgh E3 NERC doctoral training partnership grant (NE/L002558/1). P.T was also partly supported by the Global Geological Risk Platform of the British Geological Survey NC-ODA grant NE/R000069/1: Geoscience for Sustainable Futures. We thank the reviewers for their detailed and constructive reviews which have significantly improved an earlier version of this manuscript, as well as efficient editorial handling by Jamie Farquharson.

Data Availability

All data generated or analysed during this study are included in this published article and its supplementary information files.

Copyright Notice

References

Ablay, G. J., G. G. Ernst, J. Marti, and R. S. Sparks (1995). "The ~2 ka subplinian eruption of Montaña Blanca, Tenerife". *Bulletin of Volcanology* 57(5), pages 337–355. DOI: 10.1007/BF00301292.

Benvenuti, M., S. Carnicelli, G. Ferrari, and M. Sagri (2009). "Depositional Processes in Latest Pleistocene and Holocene Ephemeral Streams of the Main Ethiopian Rift (Ethiopia)". *Fluvial Sedimentology VII*. ISBN: 9781444304350, pages 277–294. DOI: 10.1002/9781444304350.ch16.

Benvenuti, M., S. Carnicelli, G. Belluomini, N. Dainelli, S. Di Grazia, G. A. Ferrari, C. Iasio, M. Sagri, D. Ventra, B. Atnafu, and S. Kebede (2002). "The Ziway-Shala lake basin (main Ethiopian rift, Ethiopia): A revision of basin evolution with special reference to the Late Quaternary". *Journal of African Earth Sciences* 35(2). ISBN: 0899-5362, pages 247–269. DOI: 10.1016/S0899-5362(02)00036-2.

Bohrson, W. A. and M. R. Reid (1997). "Genesis of silicic peralkaline volcanic rocks in an ocean island setting by crustal melting and open-system processes: Socorro Island, Mexico". *Journal of Petrology* 38(9). ISBN: 0022-3530, pages 1137–1166. DOI: 10.1093/petroj/38.9.1137.

Bonadonna, C. and B. F. Houghton (2005). "Total grain-size distribution and volume of tephra-fall deposits". *Bulletin of Volcanology* 67(5). ISBN: 0044500403862, pages 441–456. DOI: 10.1007/s00445-004-0386-2.

Branney, M. J. and P. Kokelaar (2002). *Pyroclastic density currents and the sedimentation of ignimbrites*. Volume 27. Publication Title: Geological Society London, Memoirs. Geological Society of London Special Publications. ISBN: 1-86239-097-5.

Branney, M. J. and P. Kokelaar (1992). "A reappraisal of ignimbrite emplacement: progressive aggradation and changes from particulate to non-particulate flow during emplacement of high grade ignimbrite". *Bulletin of Volcanology* 54, pages 504–520. DOI: 10.1007/BF00301396.

Brown, R. J., T. L. Barry, M. J. Branney, M. S. Pringle, and S. E. Bryan (2003). "The Quaternary pyroclastic succession of southeast Tenerife, Canary Islands: Explosive eruptions, related caldera subsidence, and sector collapse". *Geological Magazine* 140(3), pages 265–288. DOI: 10.1017/S0016756802007252.

Brown, R. J., M. J. Branney, C. Maher, and P. Dávila-Harris (2010). "Origin of accretionary lapilli within ground-hugging density currents: Evidence from pyroclastic couplets on Tenerife". *Bulletin of the Geological Society of America* 122(1). ISBN: 0016-7606, pages 305–320. DOI: 10.1130/B26449.1.

Bryan, W. B. (1966). "History and mechanism of eruption of soda-rhyolite and alkali basalt, Socorro Island, Mexico". *Bulletin Volcanologique* 29(1), pages 453–479. DOI: 10.1007/BF02597169.

Burgisser, A. and J. E. Gardner (2006). "Using hydraulic equivalences to discriminate transport processes of volcanic flows". *Geology* 34(3), pages 157–160. DOI: 10.1130/G21942.1.

Carazzo, G., S. Tait, A. Michaud-Dubuy, A. Fries, and E. Kaminski (2020). "Transition from stable column to partial collapse during the 79 cal CE P3 Plinian eruption of Mt. Pelée volcano (Lesser Antilles)". *Journal of Volcanology and Geothermal Research* 392. Publisher: Elsevier B.V. DOI: 10.1016/j.jvolgeores.2019.106764.

Castro, J. M., I. N. Bindeman, H. Tuffen, and C. Ian Schipper (2014). "Explosive origin of silicic lava: Textural and delta D-H2O evidence for pyroclastic degassing during rhyolite effusion". *Earth and Planetary Science Letters* 405. Publisher: Elsevier B.V. ISBN: 0012-821X, pages 52–61. DOI: 10.1016/j.epsl.2014.08.012.

Clarke, A. B., T. Esposti Ongaro, and A. Belousov (2015). "Chapter 28 - Vulcanian Eruptions". *The Encyclopedia of Volcanoes (Second Edition)*. Edited by H. Sigurdsson. Amsterdam: Academic Press, pages 505–518. ISBN: 978-0-12-385938-9.

Clarke, B. (2020). "Post-caldera eruptions and pyroclastic density current hazard in the Main Ethiopian Rift". PhD thesis. University of Edinburgh. 329 pages.

Clarke, B., P. Tierz, E. Calder, and G. Yirgu (2020). "Probabilistic Volcanic Hazard Assessment for Pyroclastic Density Currents From Pumice Cone Eruptions at Aluto Volcano, Ethiopia". *Frontiers in Earth Science* 8(348), pages 1–19. DOI: 10.3389/feart.2020.00348.

Clarke, B., E. S. Calder, F. Dessalegn, K. Fontijn, J. A. Cortés, M. Naylor, I. Butler, W. Hutchison, and G. Yirgu (2019). "Fluidal pyroclasts reveal the intensity of peralkaline rhyolite pumice cone eruptions". *Nature Communications* 10(1). Publisher: Springer US, pages 1–10. DOI: 10.1038/s41467-019-09947-8.

Colby, D. J., D. M. Pyle, K. Fontijn, T. A. Mather, A. A. Melaku, M. A. Mengesha, and G. Yirgu (2022). "Stratigraphy and eruptive history of Corbetti Caldera in the Main Ethiopian Rift". *Journal of Volcanology and Geothermal Research* 428, page 107580. DOI: 10.1016/j.jvolgeores.2022.107580.

Cole, J. W. (1978). "Tectonic setting of Mayor Island volcano (Note)". *New Zealand Journal of Geology and Geophysics* 21(5), pages 645–647. DOI: 10.1080/00288306.1978.10424091.

Cole, P. D., E. S. Calder, R. S. Sparks, A. B. Clarke, T. H. Druitt, S. R. Young, R. A. Herd, C. L. Harford, and G. E. Norton (2002). "Deposits from dome-collapse and fountain-collapse pyroclastic flows at Soufrière Hills Volcano, Montserrat". *Geological Society Memoir* 21(1), pages 231–262. DOI: 10.1144/GSL.MEM.2002.021.01.11.

Cole, P. D., G. Queiroz, N. Wallenstein, J. L. Gaspar, A. M. Duncan, and J. E. Guest (1995). "An historic subplinian/phreatomagmatic eruption: the 1630 AD eruption of Furnas volcano, Sao Miguel, Azores". *Journal of Volcanology and Geothermal Research* 69(1), pages 117–135. DOI: 10.1016/0377-0273(95)00033-X.

Cole, P. D., P. J. Smith, A. J. Stinton, H. M. Odbert, M. L. Bernstein, J. C. Komorowski, and R. Stewart (2014). "Vulcanian explosions at Soufrière Hills Volcano, Montserrat between 2008 and 2010". *Geological Society, London, Memoirs* 39(1), pages 93–111. DOI: 10.1144/m39.5.

Collins, B. D. and T. Dunne (1986). "Erosion of tephra from the 1980 eruption of Mount St. Helens". *GSA Bulletin* 97(7), pages 896–905. DOI: 10.1130/0016-7606(1986)97<896:EOTFTE>2.0.CO;2.

Cowlyn, J., B. M. Kennedy, D. M. Gravley, and S. J. Cronin (2020). "A Confidence-Based Assessment Method for Distinguishing Pyroclastic Density Current Deposits From Other Volcaniclastic Units". *Frontiers in Earth Science* 8. DOI: 10.3389/feart.2020.581195.

Davì, M., R. De Rosa, P. Donato, and R. Sulpizio (2011). "The Lami pyroclastic succession (Lipari, Aeolian Islands): A clue for unravelling the eruptive dynamics of the Monte Pilato rhyolitic pumice cone". *Journal of Volcanology and Geothermal Research* 201(1). Publisher: Elsevier B.V., pages 39–52. DOI: 10.1016/j.jvolgeores.2010.09.010.

Dawson, J. B. and D. G. Powell (1969). "The natron-engaruka explosion crater area, northern tanzania". *Bulletin Volcanologique* 33(3), pages 791–817. DOI: 10.1007/BF02596750.

Dellino, P. and L. L. Volpe (1995). "Fragmentation versus transportation mechanisms in the pyroclastic sequence of Monte Pilato-Rocche Rosse (Lipari, Italy)". *Journal of Volcanology and Geothermal Research* 64(3). ISBN: 0377-0273, pages 211–231. DOI: 10.1016/0377-0273(94)00084-T.

Di Genova, D., C. Romano, K. U. Hess, A. Vona, B. T. Poe, D. Giordano, D. B. Dingwell, and H. Behrens (2013). "The rheology of peralkaline rhyolites from Pantelleria Island". *Journal of Volcanology and Geothermal Research* 249. Publisher: Elsevier B.V. ISBN: 0962-8452, pages 201–216. DOI: 10.1016/j.jvolgeores.2012.10.017.

Dingwell, D. B., K. U. Hess, and C. Romano (1998). "Extremely fluid behavior of hydrous peralkaline rhyolites". *Earth and Planetary Science Letters* 158(1). ISBN: 0012821X, pages 31–38. DOI: 10.1016/S0012-821X(98)00046-6.

Doronzo, D. M., G. A. Valentine, P. Dellino, and M. D. de Tullio (2010). "Numerical analysis of the effect of topography on deposition from dilute pyroclastic density currents". *Earth and Planetary Science Letters* 300(1). Publisher: Elsevier B.V., pages 164–173. DOI: 10.1016/j.epsl.2010.10.003.

Dowey, N. and R. Williams (2022). "Simultaneous fall and flow during pyroclastic eruptions: A novel proximal hybrid facies". *Geology* 50(10), pages 1187–1191. DOI: 10.1130/G50169.1.

Druitt, T. H. (1995). "Settling behaviour of concentrated dispersions and some volcanological applications". *Journal of Volcanology and Geothermal Research* 65(1), pages 27–39. DOI: 10.1016/0377-0273(94)00090-4.

Ewart, A., S. R. Taylor, and A. C. Capp (1968). "Geochemistry of the pantellerites of Mayor Island, New Zealand". *Contributions to Mineralogy and Petrology* 17(2), pages 116–140. DOI: 10.1007/BF00373205.

Fazzini, M., C. Bisci, and P. Billi (2015). "Landscapes and Landforms of Ethiopia". *Landscapes and Landforms of Ethiopia*. Edited by P. Billi. ISSN: 2213-2090. Springer Science & Buisness Media, pages 65–87. ISBN: 978-94-017-8025-4. DOI: 10.1007/978-94-017-8026-1.

Fierstein, J., B. F. Houghton, C. J. Wilson, and W. Hildreth (1997). "Complexities of plinian fall deposition at vent: An example from the 1912 Novarupta eruption (Alaska)". *Journal of Volcanology and Geothermal Research* 76(3), pages 215–227. DOI: 10.1016/S0377-0273(96)00081-9.

Fontijn, K., K. McNamara, A. Zafu Tadesse, D. M. Pyle, F. Dessalegn, W. Hutchison, T. A. Mather, and G. Yirgu (2018). "Contrasting styles of post-caldera volcanism along the Main Ethiopian Rift: Implications for contemporary volcanic hazards". *Journal of Volcanology and Geothermal Research* 356. Publisher: Elsevier B.V, pages 90–113. DOI: 10.1016/j.jvolgeores.2018.02.001.

Forni, F., F. Lucchi, A. Peccerillo, C. A. Tranne, P. L. Rossi, and M. L. Frezzotti (2013). "Stratigraphy and geological evolution of the Lipari volcanic complex (central Aeolian archipelago)". *Geological Society, London, Memoirs* 37(1). ISBN: 9781862393653, pages 213–279. DOI: 10.1144/M37.10.

Foster, A., F. B. Wadsworth, H. Tuffen, H. E. Unwin, and M. C. S. Humphreys (2024). "Evidence for the formation of silicic lava by pyroclast sintering". *Nature Communications* 15(1), page 5347. DOI: 10.1038/s41467-024-49601-6.

Glicken, H. (1991). "Sedimentary Architecture of Large Volcanic-Debris Avalanches". *Sedimentation in volcanic settings*. Volume 45. Special Publications of SEPM. ISBN: 0-918985-89-7.

Gottsmann, J. and D. B. Dingwell (2002). "The thermal history of a spatter-fed lava flow: the 8-ka pantellerite flow of Mayor Island, New Zealand". *Bulletin of Volcanology* 64(6), pages 410–422. DOI: 10.1007/s00445-002-0220-7.

Graettinger, A. H., G. A. Valentine, and I. Sonder (2015). "Circum-crater variability of deposits from discrete, laterally and vertically migrating volcanic explosions: Experimental evidence and field implications". *Journal of Volcanology and Geothermal Research* 308. Publisher: Elsevier B.V., pages 61–69. DOI: 10.1016/j.jvolgeores.2015.10.019.

Hernando, I. R., I. A. Petrinovic, L. D'Elia, S. Guzmán, and G. N. Páez (2019). "Post-caldera pumice cones of the Payún Matrú caldera, Payenia, Argentina: Morphology and deposits characteristics". *Journal of South American Earth Sciences* 90 (November 2018). Publisher: Elsevier, pages 453–462. DOI: 10.1016/j.jsames.2018.12.017.

Higgins, M. W. (1969). "Airfall ash and pumice lapilli deposits from central pumice cone, Newberry Caldera, Oregon". *United States Geological Survey Professional Paper* 650-D. Publisher: United States Geological Survey, pages D26–D32.

– (1973). "Petrology of Newberry Volcano, Central Oregon". *Bulletin of the Geological Society of America* 84(2), pages 455–488. DOI: 10.1130/0016-7606(1973)84<455:PONVCO>2.0.CO;2.

Hildreth, W. and R. E. Drake (1992). "Volcan Quizapu, Chilean Andes". *Bulletin of Volcanology* 54, pages 93–125. DOI: 10.1007/BF00278002.

Houghton, B. F., S. D. Weaver, C. J. Wilson, and M. A. Lanphere (1992). "Evolution of a Quaternary peralkaline volcano: Mayor Island, New Zealand". *Journal of Volcanology and Geothermal Research* 51(3), pages 217–236. DOI: 10.1016/0377-0273(92)90124-V.

Houghton, B. F., C. J. Wilson, J. Fierstein, and W. Hildreth (2004). "Complex proximal deposition during the Plinian eruptions of 1912 at Novarupta, Alaska". *Bulletin of Volcanology* 66(2), pages 95–133. DOI: 10.1007/s00445-003-0297-7.

Houghton, B. F. and C. J. Wilson (1989). "A vesicularity index for pyroclastic deposits". *Bulletin of Volcanology* 51, pages 451–462. DOI: 10.1007/BF01078811.

Houghton, B. F., C. J. Wilson, and S. Weaver (1985). "Strombolian deposits at Mayor Island: "Basaltic" eruption styles displayed by a peralkaline rhyolitic volcano". *New Zealand Geological Survey record* 8, pages 42–51.

Hughes, E. C., D. A. Neave, K. J. Dobson, P. J. Withers, and M. Edmonds (2017). "How to fragment peralkaline rhyolites: Observations on pumice using combined multi-scale 2D and 3D imaging". *Journal of Volcanology and Geothermal Research* 336. Publisher: Elsevier B.V, pages 179–191. DOI: 10.1016/j.jvolgeores.2017.02.020.

Hunt, J. A., D. M. Pyle, and T. A. Mather (2019). "The Geomorphology, Structure, and Lava Flow Dynamics of Peralkaline Rift Volcanoes From High-Resolution Digital Elevation Models". *Geochemistry, Geophysics, Geosystems* 20(3), pages 1508–1538. DOI: 10.1029/2018GC008085.

Hunt, J. A., A. Zafu, T. A. Mather, D. M. Pyle, and P. H. Barry (2017). "Spatially Variable CO2 Degassing in the Main Ethiopian Rift: Implications for Magma Storage, Volatile Transport, and Rift-Related Emissions". *Geochemistry, Geophysics, Geosystems* 18(10), pages 3714–3737. DOI: 10.1002/2017GC006975.

Hutchison, W., R. Fusillo, D. M. Pyle, T. A. Mather, J. D. Blundy, J. Biggs, G. Yirgu, B. E. Cohen, R. A. Brooker, D. N. Barfod, and A. T. Calvert (2016a). "A pulse of mid-Pleistocene rift volcanism in Ethiopia at the dawn of modern humans". *Nature Communications* 7. Publisher: Nature Publishing Group ISBN: 2041-1723 (Electronic) 2041-1723 (Linking), pages 1–12. DOI: 10.1038/ncomms13192.

Hutchison, W., T. A. Mather, D. M. Pyle, J. Biggs, and G. Yirgu (2015). "Structural controls on fluid pathways in an active rift system: A case study of the Aluto volcanic complex". *Geosphere* 11(3). ISBN: 1553-040X, pages 542–562. DOI: 10.1130/GES01119.1.

Hutchison, W., D. M. Pyle, T. A. Mather, J. Biggs, and G. Yirgu (2014). *2012 Aluto LiDAR data*. DOI: 10.6084/m9.figshare.1261646.v2.

Hutchison, W., D. M. Pyle, T. A. Mather, G. Yirgu, J. Biggs, B. E. Cohen, D. N. Barfod, and E. Lewi (2016b). "The eruptive history and magmatic evolution of Aluto volcano: new insights into silicic peralkaline volcanism in the Ethiopian rift". *Journal of Volcanology and Geothermal Research* 328. Publisher: The Authors, pages 9–33. DOI: 10.1016/j.jvolgeores.2016.09.010.

Iddon, F. and M. Edmonds (2020). "Volatile-rich magmas distributed through the upper crust in the Main Ethiopian Rift". *Geochemistry, Geophysics, Geosystems*. ISBN: 0000000312431. DOI: 10.1029/2019GC008904.

Inman, D. (1952). "Measures for describing the size distribution of sediments". *Journal of Sedimentary Petrology* 22(3), pages 125–145. DOI: 10.1306/D42694DB-2B26-11D7-8648000102C1865D.

Kieffer, S. W., E. Meiburg, J. Best, and J. Austin (2021). "The mysterious grooves of Volcán Bárcena: a review of the role of streamwise counter-rotating vortices during erosion by dilute pyroclastic density currents". *Bulletin of Volcanology* 83(4), page 26. DOI: 10.1007/s00445-021-01440-9.

Kokelaar, B. P. (1983). "The mechanism of Surtseyan volcanism." *Journal of the Geological Society* 140(6), pages 939–944. DOI: 10.1144/gsjgs.140.6.0939.

Lara, L. E., J. A. Naranjo, and H. Moreno (2004). "Rhyodacitic fissure eruption in Southern Andes (Cordón Caulle; 40.5°S) after the 1960 (Mw:9.5) Chilean earthquake: A structural interpretation". *Journal of Volcanology and Geothermal Research* 138(1), pages 127–138. DOI: 10.1016/j.jvolgeores.2004.06.009.

Lorenz, V. (1974). "Vesiculated tuffs and associated features". *Sedimentology* 21(2), pages 273–291. DOI: 10.1111/j.1365-3091.1974.tb02059.x.

Lowenstern, J. B., M. A. Clynne, and T. D. Bullen (1997). "Comagmatic A-type granophyre and rhyolite from the Alid volcanic center, eritrea, northeast Africa". *Journal of Petrology* 38(12), pages 1707–1721. DOI: 10.1093/petroj/38.12.1707.

Mahood, G. (1984). "Pyroclastic rocks and calderas associated with strongly peralkaline magmatism". *Journal of Geophysical Research* 89 (B10), pages 8540–8552. DOI: 10.1029/JB089iB10p08540.

Mahood, G., C. M. Gilbert, and I. Carmichael (1985). "Peralkaline and metaluminous mixed-liquid ignimbrites of the Guadalajara region, Mexico". *Journal of Volcanology and Geothermal Research* 25, pages 259–271. DOI: 10.1016/0377-0273(85)90016-2.

Mahood, G. and W. Hildreth (1986). "Geology of the peralkaline volcano at Pantelleria, Strait of Sicily". *Bulletin of Volcanology* 48, pages 143–172. DOI: 10.1007/BF01046548.

Martin, U. and K. Németh (2006). "How Strombolian is a "Strombolian" scoria cone ? Some irregularities in scoria cone architecture from the Transmexican Volcanic Belt, near Volcan Ceboruco, (Mexico) and Al Haruj (Libya)". *Journal of Volcanology and Geothermal Research* 155, pages 104–118. DOI: 10.1016/j.jvolgeores.2006.02.012.

Mattsson, H. B. and B. A. Tripoli (2011). "Depositional characteristics and volcanic landforms in the Lake Natron-Engaruka monogenetic field, northern Tanzania". *Journal of Volcanology and Geothermal Research* 203(1). Publisher: Elsevier B.V., pages 23–34. DOI: 10.1016/j.jvolgeores.2011.04.010.

McGetchin, T. R., M. Settle, and B. A. Chouet (1974). "Cinder cone growth modeled after Northeast Crater, Mount Etna, Sicily". *Journal of Geophysical Research* 79(23). ISBN: 0148-0227, pages 3257–3272. DOI: 10.1029/JB079i023p03257.

McNamara, K., K. V. Cashman, A. C. Rust, K. Fontijn, F. Chalié, E. L. Tomlinson, and G. Yirgu (2018). "Using Lake Sediment Cores to Improve Records of Volcanism at Aluto Volcano in the Main Ethiopian Rift". *Geochemistry, Geophysics, Geosystems* 19(9), pages 3164–3188. DOI: 10.1029/2018GC007686.

Melosh, H. J. (1987). "The mechanics of large rock avalanches". *Debris Flows/Avalanches*. Edited by J. E. Costa and G. F. Wieczorek. Volume 7. Geological Society of America, page 0. ISBN: 978-0-8137-5807-7.

Mosley, M. P. and D. S. Tindale (1985). "Sediment variability and bed material sampling in gravel-bed rivers". *Earth Surface Processes and Landforms* 10(5), pages 465–482. DOI: 10.1002/esp.3290100506.

NASA (2014). *NASA Shuttle Radar Topography Mission Global 1 arc second V003*. DOI: 10.5067/MEASURES/SRTM/SRTMGL1.003.

Neave, D. A., G. Fabbro, R. A. Herd, C. M. Petrone, and M. Edmonds (2012). "Melting, differentiation and degassing at the pantelleria volcano, Italy". *Journal of Petrology* 53(3). ISBN: 0022-3530, pages 637–663. DOI: 10.1093/petrology/egr074.

Németh, K., C. Risso, F. Nullo, and G. Kereszturi (2011). "The role of collapsing and cone rafting on eruption style changes and final cone morphology: Los Morados scoria cone, Mendoza, Argentina". *Central European Journal of Geosciences* 3(2), pages 102–118. DOI: 10.2478/s13533-011-0008-4.

Orsi, G., L. Ruvo, and C. Scarpati (1989). "The Serra della Fastuca Tephra at Pantelleria: Physical parameters for an explosive eruption of peralkaline magma". *Journal of Volcanology and Geothermal Research* 39(1), pages 55–60. DOI: 10.1016/0377-0273(89)90020-6.

Pedrazzi, D., X. Bolós, and J. Martí (2014). "Phreatomagmatic volcanism in complex hydrogeological environments: La Crosa de Sant Dalmai maar (Catalan Volcanic Zone, NE Spain)". *Geosphere* 10(1), pages 170–184. DOI: 10.1130/GES00959.1.

Pierson, T. C. and J. E. Costa (1987). "A rheologic classification of subaerial sediment-water flows". *Debris Flows/Avalanches*. Edited by J. E. Costa and G. F. Wieczorek. Volume 7. Geological Society of America, page 0. ISBN: 978-0-8137-5807-7.

Pierson, T. C. and K. M. Scott (1985). "Downstream Dilution of a Lahar: Transition From Debris Flow to Hyperconcentrated Streamflow". *Water Resources Research* 21(10). ISBN: 0043-1397, pages 1511–1524. DOI: 10.1029/WR021i010p01511.

Pioli, L., E. Erlund, E. Johnson, K. Cashman, P. Wallace, M. Rosi, and H. Delgado Granados (2008). "Explosive dynamics of violent Strombolian eruptions: The eruption of Parícutin Volcano 1943-1952 (Mexico)". *Earth and Planetary Science Letters* 271(1). ISBN: 0012-821X, pages 359–368. DOI: 10.1016/j.epsl.2008.04.026.

Pyle, D. M. (1989). "The thickness, volume and grainsize of tephra fall deposits". *Bulletin of Volcanology* 51, pages 1–15. DOI: 10.1007/BF01086757.

Rapprich, V., V. Žáček, K. Verner, V. Erban, T. Goslar, Y. Bekele, F. Legesa, T. Hroch, and P. Hejtmánková (2016). "Wendo Koshe Pumice: The latest Holocene silicic explosive eruption product of the Corbetti Volcanic System (Southern Ethiopia)". *Journal of Volcanology and Geothermal Research* 310, pages 159–171. DOI: 10.1016/j.jvolgeores.2015.12.008.

Riedel, C., G. G. Ernst, and M. Riley (2003). "Controls on the growth and geometry of pyroclastic constructs". *Journal of Volcanology and Geothermal Research* 127(1). ISBN: 0377-0273, pages 121–152. DOI: 10.1016/S0377-0273(03)00196-3.

Risica, G., M. Rosi, M. Pistolesi, F. Speranza, and M. J. Branney (2022). "Deposit-Derived Block-and-Ash Flows: The Hazard Posed by Perched Temporary Tephra Accumulations on Volcanoes; 2018 Fuego Disaster, Guatemala". *Journal of Geophysical Research: Solid Earth* 127(6). DOI: 10.1029/2021JB023699.

Rotolo, S. G., V. Agnesi, C. Conoscenti, and G. Lanzo (2017). "Pantelleria Island (Strait of Sicily): Volcanic History and Geomorphological Landscape". *Landscapes and Landforms of Italy*. Edited by M. Soldati and M. Marchetti. Cham: Springer International Publishing, pages 479–487. ISBN: 978-3-319-26194-2.

Schipper, C. I., J. M. Castro, B. M. Kennedy, B. W. Christenson, A. Aiuppa, B. Alloway, P. Forte, G. Seropian, and H. Tuffen (2019). "Halogen (Cl, F) and sulphur release during explosive, effusive, and intrusive phases of the 2011 rhyolitic eruption at Cordón Caulle volcano (Chile)". *Volcanica* 2(1), pages 73–90. DOI: 10.30909/vol.02.01.7390.

Schipper, C. I., J. M. Castro, H. Tuffen, M. R. James, and P. How (2013). "Shallow vent architecture during hybrid explosive-effusive activity at Cordon Caulle (Chile, 2011-12): Evidence from direct observations and pyroclast textures". *Journal of Volcanology and Geothermal Research* 262. ISBN: 0377-0273, pages 25–37. DOI: 10.1016/j.jvolgeores.2013.06.005.

Self, S. and R. S. Sparks (1978). "Characteristics of widespread pyroclastic deposits formed by the interaction of silicic magma and water". *Bulletin Volcanologique* 41(3), pages 196–212. DOI: 10.1007/BF02597223.

Shea, T., T. Leonhardi, T. Giachetti, A. Lindoo, J. Larsen, J. Sinton, and E. Parsons (2017). "Dynamics of an unusual cone-building trachyte eruption at Puʻu Waʻawaʻa, Hualālai volcano, Hawaiʻi". *Bulletin of Volcanology* 79(4). Publisher: Bulletin of Volcanology. DOI: 10.1007/s00445-017-1106-z.

Smith, G. A. (2000). "Recognition and significance of streamflow-dominated piedmont facies in extensional basins". *Basin Research* 12(3), pages 399–411. DOI: 10.1111/j.1365-2117.2000.00125.x.

Smith, G., P. Rowley, R. Williams, G. Giordano, M. Trolese, A. Silleni, D. R. Parsons, and S. Capon (2020). "A bedform

phase diagram for dense granular currents". *Nature Communications* 11(1). Publisher: Springer US, pages 1–11. DOI: 10.1038/s41467-020-16657-z.

Sohn, Y. K. and S. K. Chough (1993). "The Udo tuff cone, Cheju Island, South Korea: transformation of pyroclastic fall into debris fall and grain flow on a steep volcanic cone slope". *Sedimentology* 40(4), pages 769–786. DOI: 10.1111/j.1365-3091.1993.tb01359.x.

Sparks, R. (1976). "Grain size variations in ignimbrites and implications for the transport of pyroclastic flows". *Sedimentology* 23(2), pages 147–188. DOI: 10.1111/j.1365-3091.1976.tb00045.x.

Sparks, R., M. I. Bursik, S. Carey, J. Gilbert, L. Glaze, H. Sigurdsson, and A. W. Woods (1997). *Volcanic Plumes*. Chichester: Wiley. 574 pages. ISBN: 0-471-93901-3.

Sparks, R., M. Bursik, G. Ablay, R. Thomas, and S. Carey (1992). "Sedimentation of tephra by volcanic plumes. Part 2: controls on thickness and grain-size variations of tephra fall deposits". *Bulletin of Volcanology* 54, pages 685–695. DOI: 10.1007/BF00430779.

Sparks, R. and J. V. Wright (1979). "Welded air-fall tuffs". *Ash-Flow Tuffs*. Edited by C. E. Chapin and W. E. Elston. Volume 180. Geological Society of America, page 0. ISBN: 978-0-8137-2180-4.

Stevenson, R. J. and L. Wilson (1997). "Physical volcanology and eruption dynamics of peralkaline agglutinates from Pantelleria". *Journal of Volcanology and Geothermal Research* 79(1), pages 97–122. DOI: 10.1016/S0377-0273(97)00021-8.

Sumner, J. M. (1998). "Formation of clastogenic lava flows during fissure eruption and scoria cone collapse: The 1986 eruption of Izu-Oshima Volcano, eastern Japan". *Bulletin of Volcanology* 60(3). ISBN: 0258-8900, pages 195–212. DOI: 10.1007/s004450050227.

Taddeucci, J., M. Pompilio, and P. Scarlato (2004). "Conduit processes during the July-August 2001 explosive activity of Mt. Etna (Italy): Inferences from glass chemistry and crystal size distribution of ash particles". *Journal of Volcanology and Geothermal Research* 137(1), pages 33–54. DOI: 10.1016/j.jvolgeores.2004.05.011.

Tadesse, A. Z., K. Fontijn, A. A. Melaku, E. F. Gebru, V. C. Smith, E. Tomlinson, D. Barfod, P. Gopon, F. Bégué, L. Caricchi, P. Laha, H. Terryn, S. Gudbrandsson, G. Yirgu, and D. Ayalew (2022). "Eruption frequency and magnitude in a geothermally active continental rift: The Bora-Baricha-Tullu Moye volcanic complex, Main Ethiopian Rift". *Journal of Volcanology and Geothermal Research* 423. DOI: 10.1016/j.jvolgeores.2022.107471.

Tierz, P., B. Clarke, E. S. Calder, F. Dessalegn, E. Lewi, G. Yirgu, K. Fontijn, J. M. Crummy, Y. Bekele, and S. C. Loughlin (2020). "Event trees and epistemic uncertainty in long-term volcanic hazard assessment of rift volcanoes: the example of Aluto (Central Ethiopia)". *Geochemistry, Geophysics, Geosystems*. DOI: 10.1029/2020GC009219.

Valentine, G. A., D. Krier, F. V. Perry, and G. Heiken (2005). "Scoria cone construction mechanisms, Lathrop Wells volcano, southern Nevada, USA". *Geology* 33(8), page 629. DOI: 10.1130/G21459.1.

Valentine, G. A., D. J. Krier, F. V. Perry, and G. Heiken (2007). "Eruptive and geomorphic processes at the Lathrop Wells scoria cone volcano". *Journal of Volcanology and Geothermal Research* 161(1), pages 57–80. DOI: 10.1016/j.jvolgeores.2006.11.003.

Valentine, G. A. and M. R. Sweeney (2018). "Compressible Flow Phenomena at Inception of Lateral Density Currents Fed by Collapsing Gas-Particle Mixtures". *Journal of Geophysical Research: Solid Earth* 123(2), pages 1286–1302. DOI: 10.1002/2017JB015129.

Vallance, J. W. and R. M. Iverson (2015). "Lahars and Their Deposits". *The Encyclopedia of Volcanoes 2*. Edited by H. Sigurdsson, B. Houghton, S. R. McNutt, H. Rymer, and J. Sitx. London: Elsevier, pages 649–664. ISBN: 978-0-12-385938-9. DOI: 10.1016/B978-0-12-385938-9.00037-7.

Wadsworth, F. B., E. W. Llewellin, J. Vasseur, J. E. Gardner, and H. Tuffen (2020). "Explosive-effusive volcanic eruption transitions caused by sintering". *Science advances* 6(39). DOI: 10.1126/sciadv.aba7940.

Walker, G. P. (1971). "Grain-Size Characteristics of Pyroclastic Deposits". *Geology* 79(6), pages 696–714. DOI: 10.1086/627699.

Walker, G. P. L., S. Self, and L. Wilson (1984). "Tarawera 1886, New Zealand - A basaltic plinian fissure eruption". *Journal of Volcanology and Geothermal Research* 21, pages 61–78. DOI: 10.1016/0377-0273(84)90016-7.

Wallenstein, N., A. Duncan, J. E. Guest, and M. H. Almeida (2015). "Eruptive history of fogo volcano, São Miguel, Azores". *Geological Society Memoir* 44(1), pages 105–123. DOI: 10.1144/M44.8.

White, J. D. and G. A. Valentine (2016). "Magmatic versus phreatomagmatic fragmentation: Absence of evidence is not evidence of absence". *Geosphere* 12(5), pages 1478–1488. DOI: 10.1130/GES01337.1.

Williams, R., M. J. Branney, and T. L. Barry (2014). "Temporal and spatial evolution of a waxing then waning catastrophic density current revealed by chemical mapping". *Geology* 42(2), pages 107–110. DOI: 10.1130/G34830.1.

Wilson, C. J. and W. Hildreth (1998). "Hybrid fall deposits in the Bishop Tuff, California: A novel pyroclastic depositional mechanism". *Geology* 26(1), pages 7–10. DOI: 10.1130/0091-7613(1998)026<0007:HFDITB>2.3.CO;2.

Woods, A. W. (1995). "A model of vulcanian explosions". *Nuclear Engineering and Design* 155(1), pages 345–357. DOI: 10.1016/0029-5493(94)00881-X.

Zanon, V., M. Neri, and E. Pecora (2009). "Interpretation of data from the monitoring thermal camera of Stromboli volcano (Aeolian Islands, Italy)". *Geological Magazine* 146(4), pages 591–601. DOI: 10.1017/S0016756809005937.